Characterization of adaptor binding and substrate processing by VCP/p97

Thesis by
Emily E. Blythe

In Partial Fulfillment of the Requirements for the
Degree of
Doctor of Philosophy

CALIFORNIA INSTITUTE OF TECHNOLOGY
Pasadena, California

2019
Defended May 15, 2019

Emily E. Blythe
ORCID: 0000-0001-6363-2644

ACKNOWLEDGEMENTS

First, I must thank my original scientific home, the Deshaies lab. Ray Deshaies introduced me to the world of ubiquitin and challenged me to not shy away from tackling the difficult questions in the field. I appreciate his encouragement and mentorship, which have shaped the way I think about science. The Deshaies lab as a whole provided a stimulating environment, and I learned so much about biochemistry and cell biology from my colleagues. I particularly want to thank Rati Verma for sharing her extensive knowledge about Cdc48 to inform and improve my work; Jing Li for working with me on the p97/proteasome substrate projects; Ruzbeh Mosadeghi and David Sherman for their patience and wisdom when I was troubleshooting assays; and Rob Oania, Heenam Park, and Daphne Shimoda for keeping the lab running day-to-day.

My committee members—Pamela Bjorkman, David Chan, Shu-ou Shan, and Alex Varshavsky—provided crucial project and career advice, and I thank them for their support over the years. I particularly thank Shu-ou for her assistance in designing fluorescence assays.

I appreciate those at Caltech who looked out for me after Ray's departure. Kai Zinn was my official advisor, and I am thankful for his effort to get up to speed about my project. Rebecca Voorhees was my unofficial advisor, and I spent a year with her and her lab. I greatly appreciate the logistical assistance, experimental help, and career advice I received from her.

I was so lucky to have a Berkeley adoptive lab that helped me bring this thesis to completion. I am grateful to Andy Martin for taking me in and for his support and mentorship during the end of my PhD. The Martin lab was very welcoming and helped me to continue to grow as a biochemist. In particular, I must thank "Team Cdc48"—Michal Olszewski, Cameron Williams, and Stephanie Gates—for providing insightful discussion and fruitful collaboration.

Finally, I want to acknowledge my friends and family, especially my partner Andy, for their support throughout my time in graduate school.

ABSTRACT

Valosin-containing protein (VCP/p97) is an essential AAA+ ATPase that is critical to numerous important cellular pathways, such as ER-associated degradation. p97 works in concert with a repertoire of adaptor proteins to extract ubiquitylated proteins from membranes or complexes and, often, target them for degradation by the proteasome. The nature of the p97 system—dependent upon a complex network of accessory proteins and targeted to substrates that are unstable and heterogeneous—makes the mechanism of substrate processing challenging to study. Here, we developed in vitro biochemical assays to reconstitute two important steps in the p97 pathway for mechanistic study: adaptor binding and substrate processing. We showed that p97-adaptor complexes are highly dynamic, recapitulating observations made in cell lysate. Using a model p97 substrate, we demonstrated for the first time that p97 processes its substrates through unfolding, a fact long presumed but never explicitly proven. Finally, with these model systems in hand, we explored the effects of p97 mutations that cause the neurodegenerative disease multisystem proteinopathy (MSP) on p97-adaptor-substrate complexes. MSP mutations cause faster substrate unfolding, and we hypothesize that this increase is due to a higher affinity for the requisite adaptors Ufd1-Npl4. Our biochemical data presents evidence for a gain of function model for MSP pathology and suggests new avenues for treating MSP.

PUBLISHED CONTENT AND CONTRIBUTIONS

(*1*) Blythe, E., Olson, K., Chau, V., and Deshaies, R., (2017). Ubiquitin- and ATP-dependent unfoldase activity of P97/VCP•NPLOC4•UFD1L is enhanced by a mutation that causes multisystem proteinopathy. *Proceedings of the National Academy of Sciences 114*, E4380–E4388, DOI: 10.1073/pnas.1706205114,
E.E.B. designed, performed, and interpreted all experiments related to p97 and contributed to the writing and editing of the manuscript.

(*2*) Xue, L., Blythe, E., Freiberger, E., Mamrosh, J., Hebert, A., Reitsma, J., Hess, S., Coon, J., and Deshaies, R., (2016). Valosin-containing protein (VCP)–Adaptor Interactions are Exceptionally Dynamic and Subject to Differential Modulation by a VCP Inhibitor. *Molecular and Cellular Proteomics 15*, 2970–2986, DOI: 10.1074/mcp.M116.061036,
E.E.B. designed and carried out the p97-p47 FRET assay and contributed to writing the manuscript.

TABLE OF CONTENTS

LIST OF FIGURES

LIST OF TABLES

NOMENCLATURE

AAA+ ATPase. ATPases associated with diverse cellular activities.

ADP. Adenosine diphosphate.

ALS. Amyotrophic lateral sclerosis.

ATP. Adenosine triphosphate.

ATPγS. Adenosine 5-(γ-thio)triphosphate.

BSA. Bovine serum albumin.

Cryo-EM. Cryoelectron microscopy.

Cy5. Cyanine 5.

D1. First ATPase domain of p97.

D2. Second ATPase domain of p97.

DNA. Deoxyribonucleic acid.

DUB. Deubiquitinating enzyme.

E1. Ubiquitin-activating enzyme.

E2. Ubiquitin-conjugating enzyme.

E3. Ubiquitin ligase.

ERAD. Endoplasmic reticulum-associated degradation.

FRET. Fluorescence resonance energy transfer.

FTD. Frontotemporal dementia.

HEK293. Human embryonic kidney 293 cells.

IκB-α. Nuclear factor of kappa light polypeptide gene enhancer in B-cells inhibitor, alpha.

IBMPFD. Inclusion body myopathy with Paget's disease of the bone and frontotemporal dementia, also called MSP.

IP. Immunoprecipitation.

ITC. Isothermal titration calorimetry.

K11. Refers to lysine 11 on ubiquitin or describes chains of ubiquitin linked through lysine 11.

K29. Refers to lysine 29 on ubiquitin or describes chains of ubiquitin linked through lysine 29.

K48. Refers to lysine 48 on ubiquitin or describes chains of ubiquitin linked through lysine 48.

K6. Refers to lysine 6 on ubiquitin or describes chains of ubiquitin linked through lysine 6.

LDH. Lactate dehydrogenase.

MS. Mass spectrometry.

MSP. Multisystem proteinopathy, also called IBMPFD.

mTOR. Mammalian target of rapamycin.

N-domain. N-terminal domain of p97.

NADH. Nicotinamide adenine dinucleotide.

NBM. Npl4 binding motif.

NF-κB. Nuclear factor kappa-light-chain-enhancer of activated B cells.

Ni-NTA. Nickel-nitrilotriacetic acid agarose resin.

NMR. Nuclear magnetic resonance.

NPLOC4/Npl4. Nuclear protein localization protein 4, called NPLOC4 in human and Npl4 in yeast.

NSF. N-ethylmaleimide-sensitive factor.

PDB. Paget's disease of the bone.

PEP. Phosphoenolpyruvate.

PK. Pyruvate kinase.

PQC. Protein quality control.

PTM. Post-translational modification.

SEC. Size exclusion chromatography.

SEP. *Saccharomyces cerevisiae* suppressor of high-copy PP1 protein (shp1), *Drosophila melanogaster* eyes closed gene (eyc) and vertebrate p47 domain.

SPR. Surface plasmon resonance.

TAMRA. Tetramethylrhodamine.

TDP-34. Tar DNA binding protein-43.

TRITC. Tetramethylrhodamine-isothiocyanate.

Ub. Ubiquitin.

UBA. Ubiquitin-associated domain.

UBD. Ubiquitin-like domain.

UBX. Ubiquitin regulatory X domain.

UBXD1. Ubiquitin regulatory X domain-containing protein 1.

UBXD4. Ubiquitin regulatory X domain-containing protein 4.

UBXD9. Ubiquitin regulatory X domain-containing protein 9.

UFD. Ubiquitin fusion degradation.

UFD1L/Ufd1. Ubiquitin fusion degradation protein 1, called UFD1L in human and Ufd1 in yeast.

UN. Heterodimer of NPLOC4/Npl4 and UFD1L/Ufd1.

UPS. Ubiquitin proteasome system.

VAT. VCP-like ATPase from *Thermoplasma acidophilum*.

VCP. Valosin-containing protein, also called p97 or Cdc48 in yeast.

VIM. VCP-interacting motif.

VIMP. Valosin-containing protein-interacting membrane protein.

ZF. Zinc finger.

Chapter 1

INTRODUCTION TO THE AAA+ ATPASE VCP/P97

1.1 The ubiquitin-proteasome system (UPS)

Cellular processes depend upon the spatiotemporal coordination of proteins; therefore, maintenance of the proteome is critical for cell survival. Many pathways are involved in proteostasis, including protein synthesis and trafficking. The ubiquitin-proteasome system (UPS) contributes to proteostasis by controlling protein degradation. In addition to its roles in programmed cellular pathways such as signal transduction, the cell cycle, and stress response, the UPS is also responsible for protein quality control (PQC), or the clearance of damaged or misfolded proteins. The roles of the UPS and PQC underscore their importance in human health; programmed protein degradation is particularly important during development, and PQC pathways are challenged during aging (*1*, *2*). Modulators of the UPS are being developed to treat a range of diseases, including viral infections, Alzheimer's, cystic fibrosis, type II diabetes, and cancer (*1–3*).

Figure 1.1 shows a summary scheme of the UPS. The 76-amino acid protein ubiquitin (Ub)—nicknamed the "molecular kiss of death'—serves as a degradation signal for proteins targeted to the UPS. Chains of ubiquitin are appended to proteins through a ubiquitylation cascade involving three types of enzymes (*4*). First, the C-terminus of ubiquitin forms a thioester linkage with an active site cysteine in an E1 ubiquitin-activating enzyme, consuming ATP. Next, the ubiquitin is passed from the E1 enzyme to a cysteine in an E2 ubiquitin-conjugating enzyme. This charged E2 works in conjunction with an E3 ubiquitin ligase to catalyze the formation of an isopeptide bond between the C-terminus of ubiquitin and the side chain of an internal lysine in the target protein. The E2/E3 cycle is repeated to form chains of ubiquitin by adding ubiquitin instead to an internal lysine in the ubiquitin already conjugated to the target protein (*5*). Ubiquitin contains seven internal lysines and an N-terminus that can serve as acceptors for ubiquitin modification. Specific ubiquitin chain linkage types are associated with both degradative and non-degradative functions such as signaling (*6*), and chains linked through lysine 48 (K48) are most associated with degradation (*7*). Chains of four or more ubiquitins recruit the proteasome (*8*), a 2.5 MDa protein assembly that unfolds and, using three proteolytic sites, digests

target proteins into short peptides (*9*).

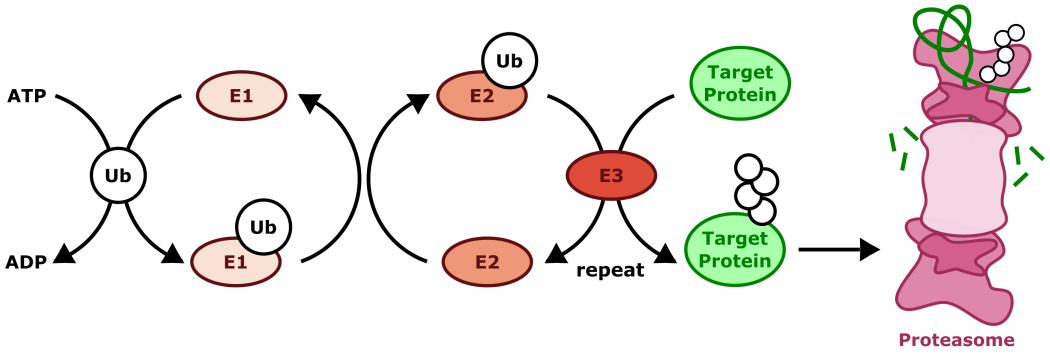

Figure 1.1: The ubiquitin proteasome system. First, the C-terminus of ubiquitin is ligated onto an active site cysteine of an E1 in an ATP-dependent manner, forming a thioester linkage. The ubiquitin is then transferred to an active site cysteine in an E2. The E2, along with an E3, transfers the ubiquitin to a lysine in the target protein, forming an isopeptide bond. The cycle repeats to build up chains of ubiquitin formed between the C-terminus of ubiquitin and an internal lysine in ubiquitin, often K48-linked. This polyubiquitin chain recruits the proteasome, which digests the target protein into peptides.

1.2 The p97 system

Sometimes proteins targeted to the UPS are in contexts that make them inaccessible to the proteasome. For example, these proteins may be embedded in a membrane or part of a large macromolecular assembly. In these cases, the cell employs p97 to aid in degradation. p97, also called valosin-containing protein (VCP) or Cdc48 in yeast, is a highly abundant AAA+ ATPase (ATPase associated with various cellular activities). p97 acts as an unfoldase and segregase, extracting and unfolding proteins to facilitate their delivery to the proteasome. Numerous cellular pathways rely on p97 activity, such as DNA repair and cell cycle control (Figure 1.2) (*10*, *11*), and the most well-studied of the p97-dependent pathways is endoplasmic reticulum-associated degradation (ERAD) (*12*). p97 also functions in some non-degradative pathways that require the action of an unfoldase or segregase, such as membrane fusion (*10*). Due to its role in the UPS, p97 is a target for cancer therapeutics, and a number of inhibitors have been developed (*3*, *13–20*).

Structurally, p97 is a homohexamer, with its subunits forming a ring around a central pore. p97 comprises three domains: an N-terminal domain (N), two ATPase domains (D1 and D2) stacked head-to-tail, and an unstructured C-terminal tail (Figure 1.3) (*22–26*). Hydrolysis of ATP by p97 generates its mechanical force from chemical energy. Each ATPase domain includes two key sequences: the Walker A motif ($GX_4GK(T/S)$, where X is any amino acid), which is responsible for nucleotide binding, and the Walker B motif ($(R/K)X_3GX_3(L/V)h_3(D/E)$, where h is

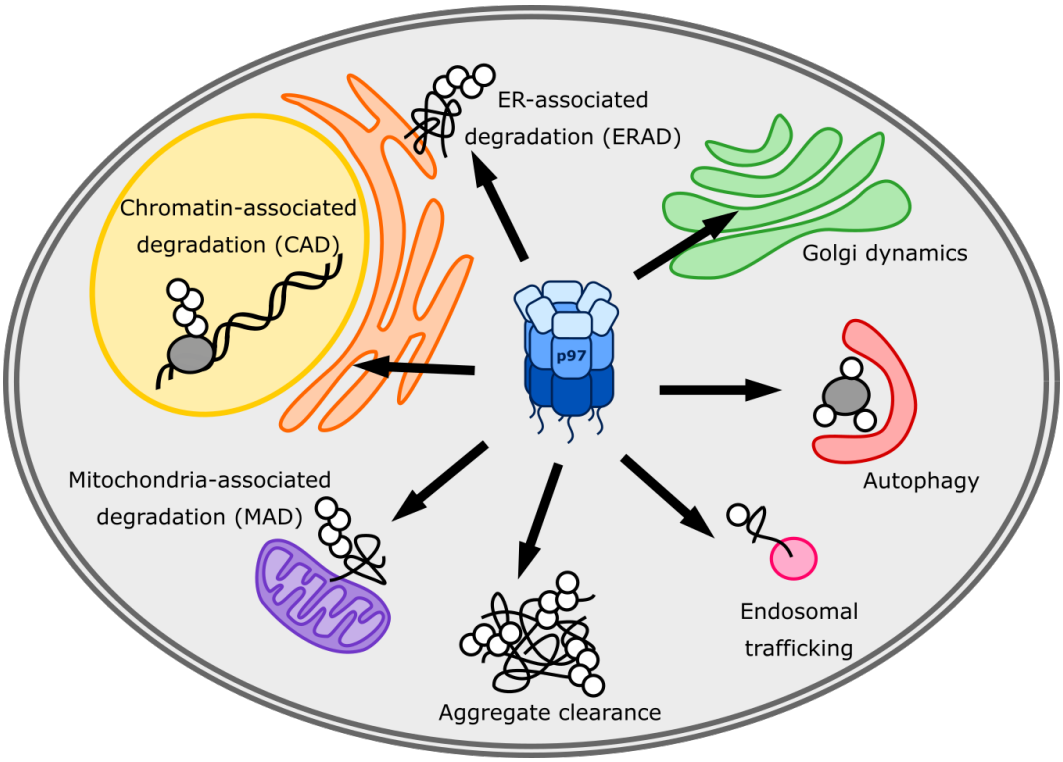

Figure 1.2: p97/VCP function. Adapted from (*21*)

any hydrophobic amino acid), which is responsible for nucleotide hydrolysis (*27*). Both D1 and D2 are competent to hydrolyze ATP, but the relative contributions of the two domains to processing substrates is controversial (*28*). D1 has a higher affinity for nucleotide while D2 has a higher hydrolysis rate, leading many to suggest that D1 plays a structural role while D2 is the main generator of force (*28–35*). Numerous structural (*22–26*, *31*, *36–43*) and biochemical (*28*, *33*, *44–47*) studies have demonstrated the extensive communication among domains during the p97 ATPase cycle. Our best understanding comes from a set of high resolution cryoelectron microscopy (cryo-EM) structures of p97 in various nucleotide states (*22*) (Figure 1.3B). When both domains are in the ADP state, the N-domain is oriented in a position planar to the D1 ring. Upon binding of ATPγS to D1, the N-domains flip upward into a position coaxial with respect to the D1-D2 barrel. D2 shows rotation with respect to the D1 upon binding of ATPγS to D2, which is in agreement with biochemical studies that suggest a flexible di-glycine linker between D1 and D2 is critical for domain communication (*45*, *46*).

p97 does not function alone but instead relies upon its interactions with adaptor proteins to provide substrate and pathway specificity (Figure 1.3A) (*48*). Many adaptors bind ubiquitin or polyubiquitin chains through ubiquitin-associated (UBA)

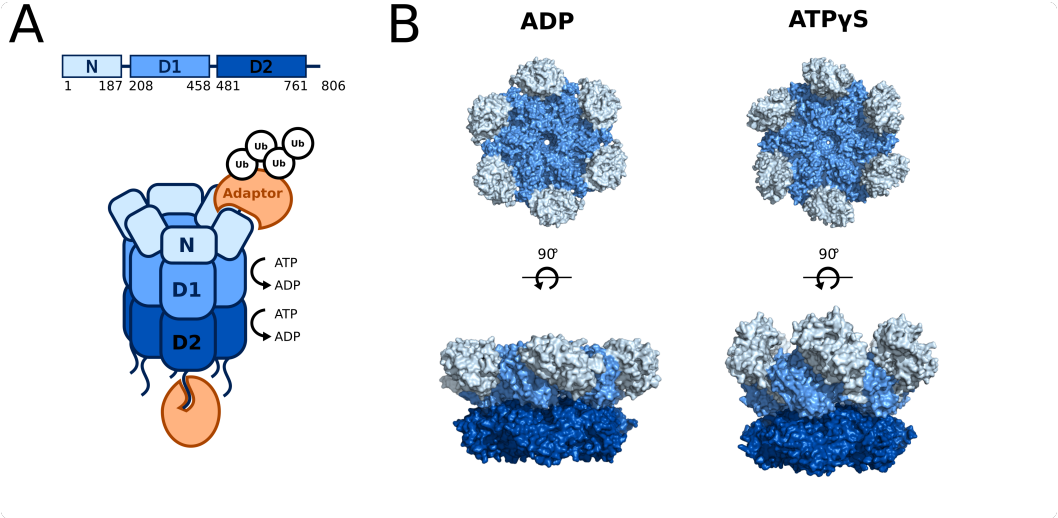

Figure 1.3: p97 structure and binding partners. (A) Cartoon representation of a p97 homohexamer showing three folded domains (N, D1, D2) as well as an unstructured C-terminal tail. Adaptor proteins (orange), many of which recruit ubiquitin, bind to the N-domains and C-terminal tails. (B) Cryo-EM structures of p97 in two nucleotide states. Upon exchange of ADP for ATPγS in both D1 and D2, the N-domains move from a coplanar to a coaxial position with respect to the D1-D2 barrel, and D2 rotates downward. PDB #5FTK and #5FTN (*22*)

domains (*49–51*) or other specialized domains (*33*, *52*), which recruit UPS substrates to p97. Other adaptors serve to process substrates through post-translational modifications (PTMs), such as addition of ubiquitin through E3 ligases, removal of ubiquitin by deubiquitinating enzymes (DUBs), or removal of oligosaccharides (*53–57*). Previous research has implicated some adaptors in specific p97 pathways (*58–62*); for example, p47 is critical for Golgi reassembly after mitosis (*63*, *64*). However, the functions of many adaptors are still unclear (*49*, *51*). Further complicating our understanding of the p97-adaptor network is the fact that some adaptors are able to co-bind p97 while other adaptors are mutually-exclusive binders (*49*, *65*, *66*).

Most adaptors bind to the N-domains or C-terminal tails of the p97 hexamer with various stoichiometries (*27*, *51*, *66*, *67*) (Figure 1.3A). Two p97 adaptors are notable exceptions and bind in unqiue ways. First, ubiquitin regulatory X domain-containing protein 9 (UBXD9) disassembles p97 hexamers to bind p97 monomers instead (*68*, *69*). Second, ubiquitin regulatory X domain-containing protein 1 (UBXD1) binds both to the N-domain and the D1-D2 barrel of p97 hexamers (*70*, *71*). A few common p97 binding motifs are employed by adaptors that bind to the N-domains. The ubiquitin regulatory X (UBX) domain, found in thirteen adaptors, interacts with the hydrophobic groove of an N-domain through an R...FPR motif (*49–51*, *72*, *73*). The VCP-interacting motif (VIM) binds to a similar surface on N-

domains using the consensus sequences $RX_5A_2X_2R$ and A_2X_2R (*71*, *74*), while the SHP motif binds to a separate site on the N-domains using the sequence $FXGXGX_2H$ (*43*, *75*).

Binding of adaptors alters the struture and activity of p97 hexamers. Low-resolution cryo-EM structures of p97 in complex with various adaptors suggest that the N-domains must be in an axial position with respect to D1-D2 for adaptors to bind to the N-domains, biasing the conformations that p97 samples (*36*, *66*, *67*, *76–78*). Adaptor binding to N-domains also propagates conformational changes to D2 (*36*, *76*). Some adaptors, such as p47, modulate ATPase activity while others, such as UN, do not (*47*, *79*, *80*).

1.3 p97 and neurodegenerative disease

Mutations in p97 have been linked to neurodegenerative diseases such as amyotrophic lateral sclerosis (ALS) and multisystem proteinopathy (MSP), also called inclusion body myopathy with Paget's disease of the bone and frontotemporal dementia (IBMPFD) (*81–83*). MSP is a fatal disease of the muscle, bone and brain that develops in middle age (reviewed in (*84*)). Myopathic symptoms include atrophy and weakness of the skeletal, cardiac, and respiratory muscles due to intracellular inclusions containing ubiquitin and other proteins such as Tar DNA binding protein-43 (TDP-43). Paget's disease of the bone (PDB) causes bone fragility and deformities due to increased osteoclast activity. Neuronal loss in the frontal and temporal lobes of the brain due to inclusions containing ubiquitin, TDP-43, and tau cause loss of reasoning, judgement, and social awareness in frontotemporal dementia (FTD). Not all MSP patients display the same symptoms. Approximately 90% of patients develop myopathy, approximately 40% of patients develop PDB, and approximately 30% of patients develop FTD; only around 10% of patients develop all three disorders (*85*). While over 50 unique missense mutations in p97 have been discovered to cause MSP (*86*), there are no strong correlations between genotype and phenotype due to the background genetic variability among individuals (*85*).

1.4 Remaining questions and research aims

While biochemical and structural studies have shed light on some of p97's general functions, many fundamental questions about p97 mechanism remain.

p97-adaptor dynamics

It remains unclear how the vast p97 network is regulated. Little is known about the dynamics of p97-adaptor association and whether other factors, such as substrates or PTMs, affect these processes (*48*). Previous work in the Deshaies lab began to answer these questions by examining p97 complexes from cells through a variety of mass spectrometry (MS) experiments (Figure 1.4)(*87*). First, the stabilities of p97-adaptor complexes were probed by immunoprecipitation (IP)-MS. Cells expressing p97 tagged at the genomic locus with the FLAG epitope were grown in isotopically "light" media while cells with untagged p97 were grown in "heavy" media. Cell lysates were incubated with anti-FLAG antibodies, and the captured proteins were assessed by MS. If the complexes are stable, only light adaptors would be captured by FLAG-p97, representing endogenous complexes. However, if the complexes are dynamic, the bound adaptors would be a 1:1 mixture of heavy and light due to exchange. As seen in Figure 1.4A, most adaptors display rapid exchange, with the notable exception of UBXD9.

To further validate these dynamics, a competition IP-MS experiment was performed. Cell lyates were spiked with increasing amounts of a truncated p97 (N-D1-L) which is competent to bind adaptors but is not recognized by the antibody used for IP. If complexes are stable, the pull-down efficiency of adaptors should be impervious to added p97-ND1L, but if complexes are unstable, the adaptors should be chased by added p97-ND1L. With the exception of UBXD9 and UBXD4, all adaptors were readily depleted in the IP by the addition of exogenous p97-ND1L, further underscoring the dynamic nature of p97-adaptor interactions (Figure 1.4B). Additionally, size exclusion chromatography (SEC)-MS was used to assess p97-adaptor complexes in cell lysate. In agreement with the other MS experiments, only UBXD4 and UBXD9 were observed to co-elute with p97, suggesting no other adaptors form stable complexes with p97 (Figure 1.4C).

A multitude of factors could influence the rapid dynamics of the p97-adaptor network in the cell (*48*). The proteins themselves could have intrinsically dynamic interactions, and these interactions could be further modulated by PTMs, oligomeric states, and conformational changes. Outside factors such as competition for binding sites or additional binding partners could also affect the network. In the previous experiments in cell lysate, it is impossible to tease apart the effects of these different influences; therefore, the first goal of this work is to probe the dynamics of the p97-adaptor network using an in vitro reconstituted system.

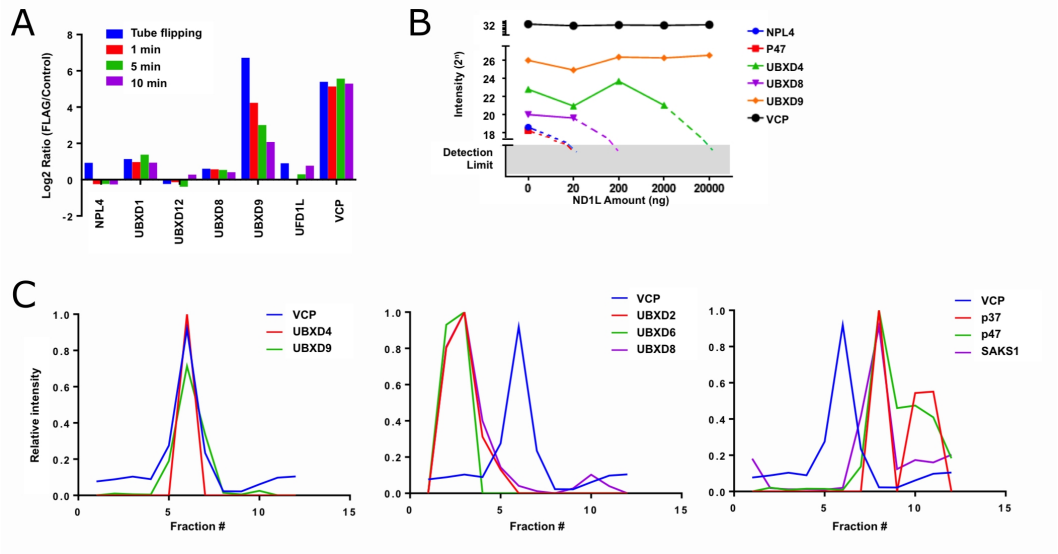

Figure 1.4: p97-adaptor network is dynamic in cell lysate. (A) Exchange rate of p97 adaptors during IP-MS. Cells expressing FLAG-p97 and WT p97 were grown in light and heavy media, respectively. Lysates were incubated with anti-FLAG antibodies for various amounts of time, and the ratio of heavy to light adaptors recovered was determined by MS. All adaptors show rapid equilibration (as evidenced by a light:heavy ratio close to 1), except UBXD9. (B) A p97 fragment, ND1L, which can bind adaptors but not the antibody used for IP, was added in increasing amounts to an IP of cell lysates, and the recovery of adaptor proteins was plotted. While the p97-UBXD9 complex is insensitive to added p97-ND1L, all other adaptors have reduced recovery as rapid exchange allows p97-ND1L to compete with full length p97 for adaptor binding. (C) Fractionation profiles in a SEC-MS experiment for a variety of p97 adaptors. Only UBXD9 and UBXD4 co-elute with p97 after fractionation on a Superose 6 sizing column. All panels are modified from data previously published (*87*).

Substrate processing by p97

Due to its functions in cellular pathways and its homology to other AAA machines such as ClpA (*88*), the proteasome 19S regulatory particle (*89*, *90*), the VCP-like ATPase from *Thermoplasma acidophilum* (VAT) (*91*, *92*), and N-ethylmaleimide-sensitive factor (NSF) (*93*), most have assumed that p97 remodels its protein substrates through unfolding. However, this function has never been explicitly demonstrated. Many AAA ATPases unfold their substrates by feeding the polypeptide through their central pores (e.g. (*94*)). However, p97 does not contain the requisite hydrophobic pore residues in its D1 domain for this threading mechanism, though other pore residues in D1 have been implicated in substrate processing (*34*, *95*). Additionally, structural studies of p97 have revealed a narrow central pore that may not be able to accommodate a threaded polypeptide (*22*, *25*). Many other mechanisms for unfolding have been proposed, such as unfolding exclusively in the D2 pore through an arginine "denaturation collar" or exclusively through the N-domain movements without direct participation of the pore, similar to that of NSF (*93*, *95*).

The special difficulties of studying p97 pathways in vitro have long stymied

research into these questions. Native p97 substrates are complex, unstable, heterogeneous, and highly modified by ubiquitin, making their purification for biochemical studies challenging. Therefore, the presumed function of p97—protein unfolding—has never been directly tested, and previous studies on p97 function have instead relied on indirect assays, such as measurements of basal ATP hydrolysis rates and reconstitutions with cellular components (e.g.(*95*)).

In addition to whether or not p97 is a bona fide unfoldase, many other fundamental questions about p97 mechanism remain unanswered. First, the minimal components necessary to reconstitute substrate processing remains obscure. It is assumed that p97 requires adaptors to recruit substrates (*48*), but p97's multitude of adaptors complicates our understanding. Though it is unclear what role each adaptor may play in substrate unfolding, a good candidate for p97's general unfolding partner is the heterodimer Ufd1/UFD1L and Npl4/NPLOC4 (UN), as this adaptor has been implicated in numerous proteasome-dependent degradative pathways such as ERAD (*10*, *65*, *96*, *97*). In particular, UN is a critical component of, and the only substrate adaptor linked to, the ubiquitin fusion degradation (UFD) pathway, a p97-dependent degradation process (*34*, *98*). ATP is also likely required for substrate processing, as ATPase activities in D1 and D2 are critical for substrate processing in cells (*34*).

Second, it is unclear what the requirements are for the substrate itself in order for it to be processed by p97. Unlike the proteasome, p97 does not require a disordered region on the substrate to initiate processing (*34*, *99*). Due to p97's role in PQC, p97-dependent processes have been connected to numerous ubiquitin linkage types, including K6, K11, K29 and K48 (*98*, *100–102*). In particular, Ufd1 binds K48-linked chains specifically, while Npl4 associates with poly-ubiquitin chains in a linkage type-independent manner (*33*, *52*, *77*). Therefore, it is likely substrates require ubiquitylation, but the linkage types and chain topologies that support proessing by p97 are undefined.

In order to address these critical gaps in our understanding of the basic biochemical activity that underlies p97's cellular functions, the second aim of this work is to develop an in vitro reconstitution of p97 substrate processing using purified components.

Perturbations caused by p97 disease mutations

The mechanism by which mutations in p97 cause neurodegenerative diseases remains highly controversial. Defects in numerous cellular pathways, such as autophagy, endosomal trafficking, lysosomal function, mitochondrial homeostasis, ERAD, mTOR regulation, energy balance, aggregate clearance, and NF-κB signaling (*58*, *84*, *103–114*), have all been reported in MSP mutants, yet the underlying cellular perturbations that cause disease pathology remains a mystery. On a more basic level, it even remains unclear whether the the molecular-level defect in these dominantly-inherited MSP mutations causes a gain or loss of p97 function. This question is particularly relevant for treatment, as many p97 inhibitors, such as NMS-873 and CB-5083, have already been developed for cancer treatment (*14*, *15*, *115*).

The majority of MSP mutations lie on the interface between the N and D1 domains (*83*), and in vitro studies have provided some clues as to the effects of these mutations on p97 structure and enzymology. Under basal conditions, MSP mutants show an increase in ATPase activity in D2 (*28*, *47*, *116–119*). The functional significance of this activity is hotly debated. Some have speculated that this higher activity is not a productive gain of function but instead represents an uncoupling of ATP hydrolysis from mechanochemical transduction in the ring due to severed communication between the regulatory N domain and the D1 ATPase domain (*83*, *120*). A dominant-negative mechanism in which non-functional mutant protomers poison the activity of WT-MSP mixed hexamers could then explain the inheritance pattern of MSP.

Structurally, mutants show an abnormal N-D1 conformation, with the N domains occupying a more axial, ATP-like conformation with respect to D1 regardless of nucleotide state due to a destabilization of ADP binding (*118*, *119*, *121–124*). IPs from cells suggest altered associations with adaptors in MSP mutants, with some adaptors being more abundant and others less (*116*, *125*). In particular, the loss of UBXD1 binding, which is linked to endosomal sorting, has been proposed as a major cause of disease (*58*, *126*).

With no biochemical assay available to directly test the effects of these mutations on p97's basic function—protein unfolding—it has been impossible to discern whether MSP mutants represent a true gain or loss of function. Therefore, the third aim of this work is to use the tools described above to explore how MSP mutations perturb adaptor binding and substrate unfolding by p97.

Chapter 2

PROBING P97-ADAPTOR INTERACTIONS BY FRET

The p97-p47 results and p97-p47 methods were previously published in: Xue, L., Blythe, E.E., Freiberger, E.C., Mamrosh, J.L., Hebert, A.S., Reitsma, J.M., Hess, S., Coon, J.J., and Deshaies, R.J. (2016) Valosin-containing protein (VCP)-adaptor interactions are exceptionally dynamic and subject to different modulation by a VCP inhibitor. *Mol Cell Proteomics* **15**, 2970-2986.

2.1 Introduction

The first goal of this work was to investigate the properties of p97-adaptor interactions in order to gain mechanistic insight into the how the incredibly dynamic p97-adaptor network is regulated. We chose two p97-adaptor pairs on which to focus. First, we developed a fluorescence resonance energy transfer (FRET) assay to quantify the interaction between p97 and p47. p47, also called NSFL1C, is involved in Golgi reassmebly after mitosis by binding to syntaxin 5 (*63*, *64*, *127*). p47 is a homotrimer comprising three domains: a UBA domain that preferentially binds mono-ubiquitin, a SEP domain that mediates trimerization, and a UXB domain (*65*, *76*, *128*) (Figure 2.1A). One p47 trimer binds one p97 hexamer through interactions between both its UBX domain and a SHP motif located in SEP-UBX linker on separate sites on the p97 N domain (*63*, *72*, *76*, *129*). p47 was an appealing target not only because its role in membrane dynamics was well established but also because a crystal structure of its UBX domain bound to p97-ND1 was published, facilitating the design of FRET probes (*72*).

Second, we focused on developing a FRET binding assay for p97-UN. Due to its participation in a wide array of p97 processes as discussed in Chaper 1, UN was an important target for this assay. Npl4 comprises a ubiquitin-like domain (UBD), which binds to the p97 N domain, and a zinc finger (ZF) domain that binds poly-ubiquitin (*65*, *130*). Ufd1 comprises a UT3 domain which binds ubiquitin, a SHP motif that binds to the p97 N domain, and an Npl4 binding motif (NDM) (*33*, *75*, *129*, *131*) (Figure 2.4A). One heterodimer of UN binds one p97 hexamer (*65*, *80*, *129*, *130*). Similar to p47, a structure of the Npl4 UBD domain bound to the p97 N domain was published, aiding in FRET assay design (*130*).

Using these designed FRET assays of p97-p47 and p97-UN, we demonstrate that the rapid dynamics of p97-adaptor complexes observed in our previous cell-based MS experiments are due to the intrinsic properties of these proteins, suggesting there is not a requirement for an exogenous factor to facilitate p97-adaptor complex assembly or disassembly. However, these rapid dynamics suggest that some stabilizing factors may exist to promote the formation of p97-adaptor complexes during cellular processes. In agreement with structural work, the affinities of these interactions are highly dependent on the nucleotide state of p97, underscoring the importance of N-domain movement for adaptor binding. Additionally, we observed enhanced binding of both p47 and UN in MSP mutants, suggesting adaptor balance defects in mutant cells may underlie some MSP pathology.

2.2 Results

p97-p47

Using the crystal structure of p47 bound to the N-domain of p97 as a guide (*72*) (Figure 2.1B), we first mutagenized the C-terminal amino acid (Thr370) of p47 to cysteine, and then reacted the purified recombinant protein with maleimide-TAMRA to generate $p47^{TAMRA}$. For p97, we used the ybbR tagging method (*132*) to attach a Cy5 tag at its N terminus (^{Cy5}p97). Upon mixing $p47^{TAMRA}$ and ^{Cy5}p97 and exciting with 540 nm light, we observed a significant reduction in TAMRA fluorescence coupled to an increase in Cy5 emission (Figure 2.2). This FRET signal was because of specific interaction of $p47^{TAMRA}$ and ^{Cy5}p97, because it was competed by addition of excess unlabeled p97 (Figure 2.2).

By titrating ^{Cy5}p97, we estimated a K_D of 65 nM for interaction of the two proteins in the absence of nucleotide (Figure 2.3A and Table 2.1). This affinity is 10-fold tighter than what was reported from isothermal titration calorimetry (ITC) studies (*50*, *76*), but is close to the affinity measured in a pair of surface plasmon resonance (SPR) studies (20–31 nM) (*133*, *134*). However, there are significant problems with measuring p47-p97 interactions by SPR because of the oligomeric nature of both proteins. In addition, none of the studies cited above addressed the crucial issue of the dynamics of p47-p97 interaction. To investigate binding dynamics, we measured the k_{on} for complex formation and k_{off} for complex dissociation in the absence of nucleotide ("apo") or in the presence of ADP or ATPγS with and without VCP inhibitors. Examples of k_{off} and k_{on} measurements in the absence of nucleotide are shown in Figures 2.3B and 2.3C, respectively, and a plot of k_{obs} versus [^{Cy5}p97] that was used to estimate k_{on} is shown in Figure

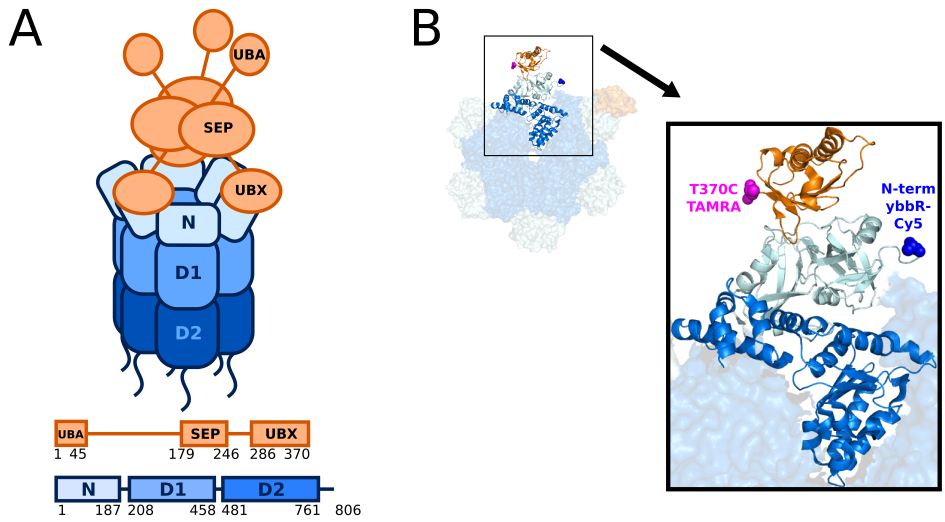

Figure 2.1: p97-p47 FRET construct design. (A) Cartoon diagram of p97 (blue) and p47 (orange) showing domain architecture. (B) Crystal structure of p47 UBX domain bound to p97-ND1, with the positions of FRET dyes labeled. A mutant p47 (T370C) was labeled with TAMRA donor dye via maleimide chemistry. p97 was labeled with an N-terminal ybbR tag to which a Cy5 acceptor dye was enzymatically conjugated. PDB#1S3S

2.3D. As shown in Table 2.1, k_{on} values were essentially invariant, ranging from 8–11x10^7 $M^{-1}sec^{-1}$ regardless of nucleotide state. Meanwhile, k_{off} showed slightly more variation, ranging from 2.5 s^{-1} in the presence of ATP and NMS-873 to 9.5 s^{-1} in the presence of ADP. Consistent with the lack of an effect of NMS-873 on co-IP of p47 with p97 from lysates (*87*), addition of NMS-873 in the presence of ATP had less than a twofold effect on k_{off} (Table 2.1). These results confirm that purified $p47^{TAMRA}$ exhibited extremely dynamic association with purified ^{Cy5}p97 in accordance with the behavior of these proteins in HEK293 cell extracts, and that their association was relatively insensitive to modulation by NMS-873.

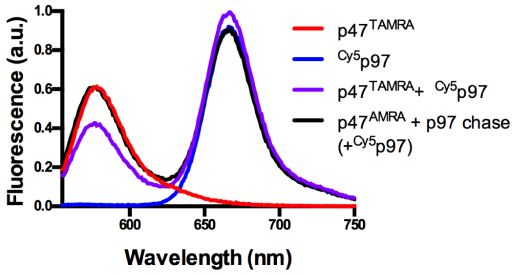

Figure 2.2: $p47^{TAMRA}$ and ^{Cy5}p97 show FRET. Fluorescence emission spectra of 16.7 nM $p47^{TAMRA}$ trimer, 83.3 nM ^{Cy5}p97 hexamer, and a mixture excited at 540 nm shows a 20% loss of TAMRA donor fluorescence in the presence of ^{Cy5}p97. Loss of fluorescence is prevented by preincubation of $p47^{TAMRA}$ with 833 nM unlabeled p97 hexamer.

p97-UN

In order to further investigate the dynamics of p97-adaptor complexes, we developed a FRET assay to probe the p97-UN complex. As shown in Figure 2.4, the N-termini of p97 and Npl4 are nearby one another. A FRET construct labeling

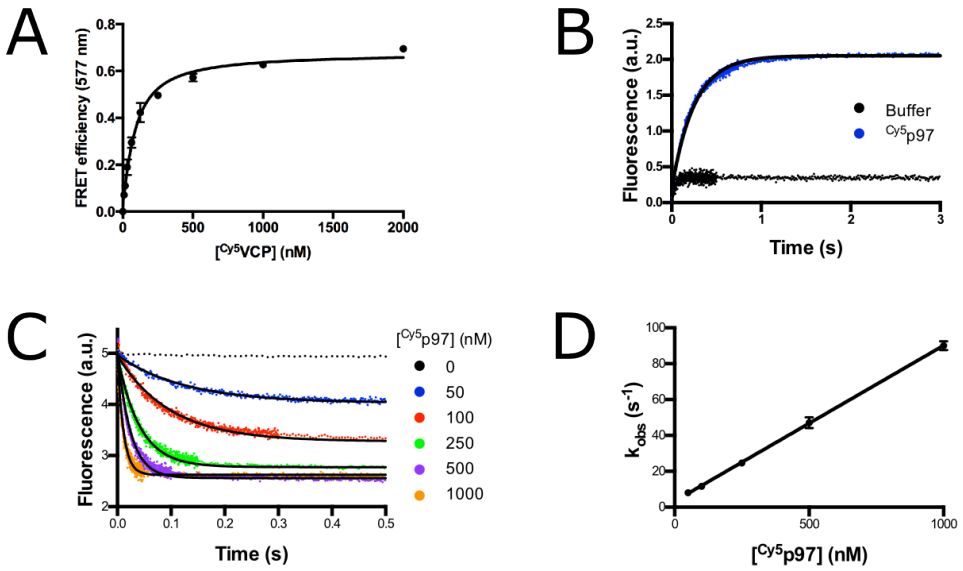

Figure 2.3: Example p97-p47 FRET data. (A) Equilibrium titration of 50 nM $p47^{TAMRA}$ trimer with ^{Cy5}p97 hexamer in the absence of nucleotide. Fit to a quadratic binding equation yields a K_D of 65 ± 7 nM. Error bars represent S.D., with n=3. (B) Change in donor fluorescence of 50 nM $p47^{TAMRA}$ trimer preincubated with 300 nM ^{Cy5}p97 hexamer upon addition of 3 μM unlabeled p97 hexamer in the absence of nucleotide. Curve was fit to a single exponential to give k_{off} of 4.04 s^{-1}. (C) Change in donor fluorescence of 50 nM $p47^{TAMRA}$ trimer upon addition of ^{Cy5}p97 hexamer at various concentrations in the absence of nucleotide. Curves were fit to a single exponential. (D) Exponential fits measured in panel (C) plotted against the concentration of ^{Cy5}p97 hexamer. Linear slope gives k_{on} of 8.68x10^7 ± 0.09x10^7 $M^{-1}s^{-1}$. Error bars represent S.D., with n=5.

	p97				p97-R155H			
Buffer	K_D (nM) (eq)	k_{on} (x10^7 $M^{-1}s^{-1}$)	k_{off} (s^{-1})	K_D (nM) (k_{off}/k_{on})	K_D (nM) (eq)	k_{on} (x10^7 $M^{-1}s^{-1}$)	k_{off} (s^{-1})	K_D (nM) (k_{off}/k_{on})
Apo	65 ± 7	8.68 ± 0.09	4.04 ± 0.09	47	49 ± 6	9.2 ± 0.1	2.496 ± 0.005	27
ATPγS	n.d.	10.5 ± 0.1	3.30 ± 0.02	31	n.d.	3.89 ± 0.08	2.04 ± 0.03	52
ADP	n.d.	8.30 ± 0.07	9.50 ± 0.08	114	n.d.	7.9 ± 0.1	3.44 ± 0.06	44
Apo + CB-5083	n.d.	8.0 ± 0.1	4.80 ± 0.03	60	n.d.	4.07 ± 0.06	2.06 ± 0.04	51
ATP + NMS-873	n.d.	11.01 ± 0.01	2.50 ± 0.03	23	n.d.	7.03 ± 0.05	1.98 ± 0.01	28

Table 2.1: Kinetic and equilibrium binding constants for $p47^{TAMRA}$-^{Cy5}p97.

the N-terminus of Npl4 with a donor TRITC fluorophore via sortase (*135*) was designed to complement the ^{Cy5}p97 used in the previously described p47-p97 FRET assay. Incubation of $U^{TRITC}N$ with ^{Cy5}p97 lead to a decrease in TRITC fluorescence, indicative of FRET (Figure 2.5). Importantly, the loss of fluorescence can be rescued by the addition of unlabeled UN, providing evidence that this FRET assay is specific (Figure 2.5).

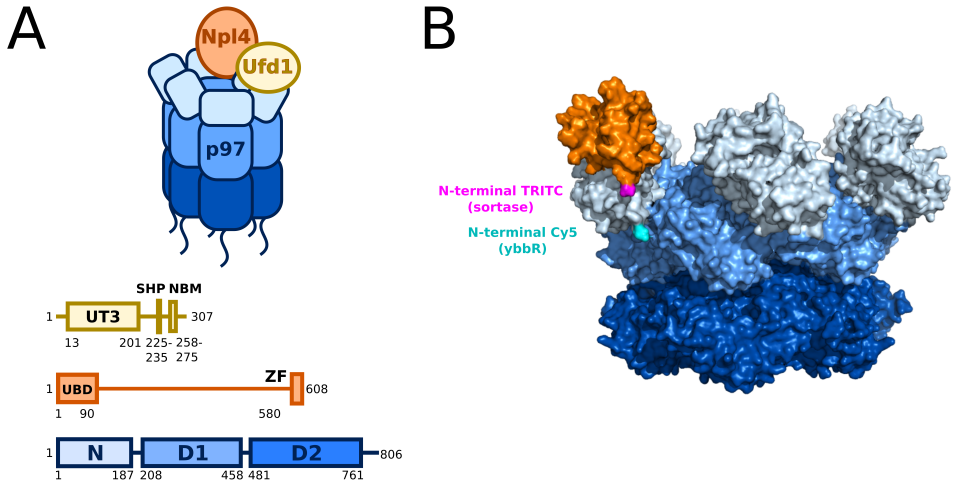

Figure 2.4: p97-UN FRET construct design. (A) Cartoon diagram of p97 (blue) and the UN heterodimer (orange and yellow, respectively) showing domain architecture. Adapted from (*75*). (B) Structure of Npl4 UBD domain bound to p97 N domain, with the positions of FRET dyes labeled. The N-terminus of Npl4 was labeled with a TRITC dye via sortase labeling, while the N-terminus of p97 was labeled with Cy5 via a ybbR tag as described above for p97-p47 FRET. Composite of PDB #2PJH and #5FTN

With this assay in hand, we were able to measure the equilibrium and kinetic constants for p97-UN in various nucleotide states (Figure 2.6, Table 2.2). The equilibrium dissociation constant is 2-fold less in ATP versus ADP and has a further reduction in ATPγS. These K_D measurements are close to that measured by SPR (100-400 μM) (*133*) but 2-10-fold tighter than that measured by ITC in the absence of nucleotide (1.7 μM) (*50*). SPR studies also observed an increase in UN affinity when p97 was in an ATP state (*133*). Due to the low affinity in ADP, we were able to measure on- and off-rates for the ATP and ATPγS states only (Table 2.2). The two conditions have similar rates, with ATPγS showing a slightly faster on-rate and slightly slower off-rate. Compared to p47, UN has a nearly 80-fold slower on-rate and 10-fold slower off-rate, suggesting that while p97-adaptor dynamics are generally rapid, variation among adaptors is present.

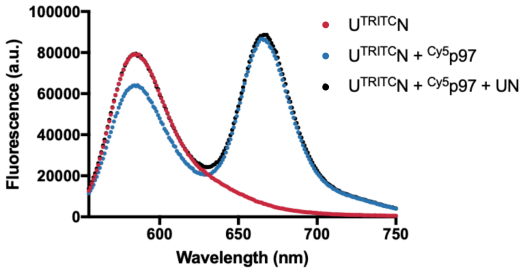

Figure 2.5: $U^{TRITC}N$ and $^{Cy5}p97$ show FRET. Fluorescence emission spectra of 50 nM $U^{TRITC}N$ heterodimer shows a 20% loss of fluorescence in the presence of 250 nM $^{Cy5}p97$ hexamer. Loss of fluorescence is prevented by addition of 2.5 μM unlabeled UN heterodimer.

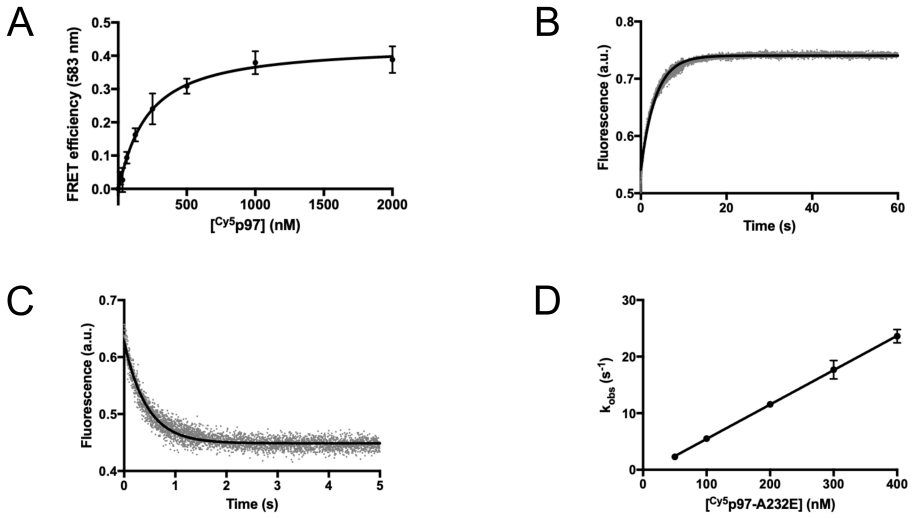

Figure 2.6: Example p97-UN FRET data. (A) Equilibrium K_D titration of 50 nM $U^{TRITC}N$ with ^{Cy5}p97 hexamer in the presence of ATPγS. Data were fit to a quadratic binding equation. Error bars represent S.D., with n=3. (B) Change in donor fluorescence of 50 nM $U^{TRITC}N$ preincubated with 250 nM ^{Cy5}p97 upon addition of 2.5 μM unlabeled UN in the in the presence of ATPγS. Curve was fit to a single exponential to give k_{off}. (C) Change in donor fluorescence of 50 nM $U^{TRITC}N$ upon addition of 50 nM ^{Cy5}p97-A232E in the presence of ATPγS. Curve was fit to a single exponential to give k_{obs}. (D) Exponential fit like those measured in panel (C) plotted against the concentration of ^{Cy5}p97-A232E. Linear slope gives k_{on}. Error bars represent S.D., with n=5.

	K_D (nM)			k_{on} (x10^6 $M^{-1}s^{-1}$)			k_{off} (s^{-1})		
p97	ATP	ADP	ATPγS	ATP	ADP	ATPγS	ATP	ADP	ATPγS
WT	302 ± 51	636 ± 96	177 ± 32	1.3 ± 0.3*	n.d.	1.9 ± 0.3*	0.48 ± 0.01	n.d.	0.33 ± 0.01
R155H	6.3 ± 0.1*	n.d.	n.d.	53 ± 1	n.d.	n.d.	0.332 ± 0.001	n.d.	n.d.
A232E	4.6 ± 0.2*	50 ± 11	4.6 ± 0.2*	54 ± 1	3.3 ± 0.7*	61 ± 1	0.25 ± 0.01	0.165 ± 0.003	0.28 ± 0.01
T262A	3.5 ± 0.1*	n.d.	n.d.	60 ± 1	n.d.	n.d.	0.210 ± 0.001	n.d.	n.d.

Table 2.2: Kinetic and equilibrium binding constants for $U^{TRITC}N$-^{Cy5}p97. Error represents S.D., with n ≥ 3. *Calculated from other values.

Effects of disease mutants on adaptor binding

Because pull-downs from cells showed differential adaptor binding in MSP mutants (*125*), we were interested in investigating how binding of p47 and UN changes in MSP mutants. For p47, we measured binding constants for the MSP mutant R155H in the presence of various nucleotides and inhibitors (Table 2.1). The largest difference we observed among all parameters was the off-rate in ADP. While WT p97 has a nearly 3-fold faster off-rate in ADP versus ATPγS, R155H retains a similar off-rate regardless of nucleotide state. This observation is in agreement with published SPR data (*136*). For UN, we measured binding constants for R155H as

well as two other mutants, A232E and T262A (Table 2.2). We characterized UN binding of A232E most fully and, as with WT p97, we observed a slower on-rate and therefore a decrease in affinity in the ADP state compared to ATP or ATPγS. Strikingly, A232E has a 10-60-fold higher UN affinity compared to WT regardless of nucleotide state, and this increase is the result of a significantly faster on-rate. R155H and T262A have very similar affinities to A232E in the presence of ATP, suggesting that this phenomenon is a common feature of MSP mutations.

Patients with MSP have one mutated allele and one WT allele, so in cells we expect mixed WT-MSP hexamers to exist. In order to probe the adaptor affinity in mixed hexamers, we devised a purification scheme to prepare mixed hexamers from *E. coli*. WT and His-tagged A232E were co-expressed, and hexamers with different WT:A232E ratios were broadly pooled into three fractions using a stepwise elution from a nickel affinity column (Ni-NTA) (Figure 2.7A). The UN affinity of 'Mixed 2' was indirectly measured by a FRET competition assay (Figure 2.7B). Briefly, $U^{TRITC}N$ and ^{Cy5}A232E were incubated with unlabeled p97 hexamers, and the inhibition of FRET was measured. The UN binding affinity K_i was then calculated from a curve fit of IC_{50} using the known concentrations and K_D for A232E-UN. As seen in Figure 2.7B, the UN affinities for pure WT and A232E hexamers agree fairly well with those measured directly (Table 2.2), and the affinity for the mixed hexamers falls in between that of the pure hexamers. No protomer exchange occurred during the time scale of the competition FRET experiment (Figure 2.7C). Therefore, the UN affinity of p97 titrates with the number of mutant subunits.

2.3 Discussion

The p97-p47 and p97-UN complexes are sensitive to the nucleotide state of p97, and that these adaptors have high affinity for p97 in an ATP-bound state is in agreement with published structural information. The N-domains of p97 adopt an "up" conformation with respect to the ATPase rings in ATP whereas they adopt a more "down" conformation in ADP (*22*). Cryo-EM structures of p97-p47 and p97-UN show the adaptors perched on top of p97, suggesting that the N-domains need to be in an "up" or ATP-bound conformation to bind adaptor (*67*, *76*, *78*).

Both complexes have altered affinities in MSP mutants, which have altered N-domain conformations. p47 binding becomes insensitive to nucleotide state with mutant p97, and the same phenomenon has been reported for two other p97 adaptors, valosin-containg protein-interacting membrane protein (VIMP) and ataxin

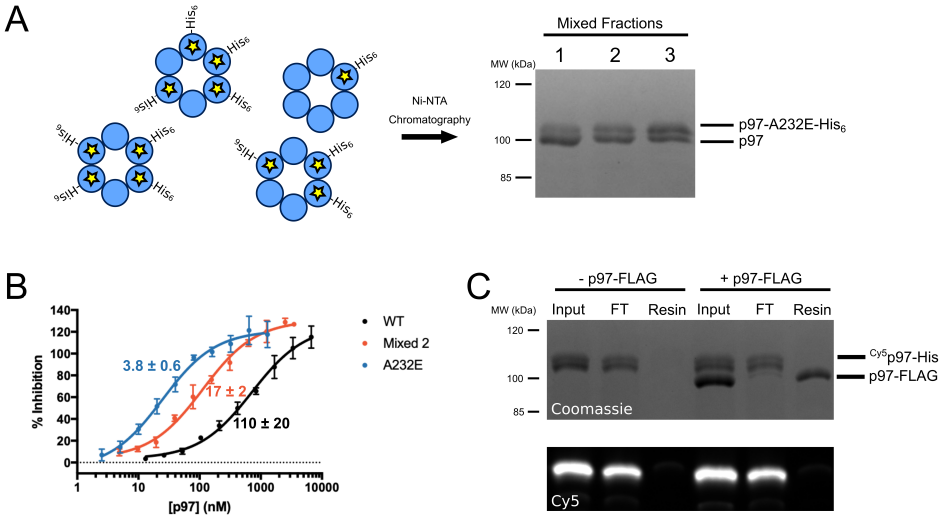

Figure 2.7: WT-A232E mixed hexamer purification and FRET (A) Mixed hexamer purification scheme. WT and A232E-His were co-expressed in *E. coli*, and three fractions of mixed hexamers with increasing amounts of A232E protomers were crudely purified by stepwise elution from a Ni-NTA column. (B) Competition FRET assay of 25 nM $U^{TRITC}N$-^{Cy5}A232E by unlabeled p97 in the presence of ATP. K_i was calculated from a curve fit of IC_{50} using the known K_D for A232E. Error bars represent S.D., with n=3. (C) Protomer exchange is slow. ^{Cy5}p97-His was incubated with anti-FLAG resin in the presence or absence of p97-FLAG for ten minutes. Coomassie stain and fluorescence scan of an SDS-PAGE gel show no evidence of ^{Cy5}p97-His binding to the resin despite robust binding of p97-FLAG.

(*124*, *137*). UN behaves differently, showing increased affinity for mutant p97 under all nucleotide conditions. Structural studies have consistently shown than MSP mutants favor N-domains in an up conformation even in ADP (*118*, *121*, *123*, *138*), which would explain why adaptors are able to maintain high affinity interactions in ADP with mutant p97. Nuclear magnetic resonance (NMR) studies measuring the dynamics of N domain movements suggest that WT and mutant p97 have similar up/down equilibrium in ATPγS (*121*). We still observe a large difference in UN affinity under those conditions, which would suggest instead that differences in up/down dynamics remain regardless of nucleotide state. Alternatively, MSP mutations could be altering p97 structure beyond its normal up/down movement that further promotes UN binding. NMR studies with mixed WT and mutant hexamers demonstrated cooperativity in N domain orientation among adjacent protomers, which implies that adaptor affinity in mixed hexamers is not linearly related to the number of mutant protomers (*123*). Our biochemical data is consistent with differential adaptor binding to WT versus mutant p97 in IPs from cell lysate, though the rapid exchange of these factors suggest these interactions were formed in lysate rather than originating in the cell (*116*, *125*). The significance of these findings to MSP pathology remains unclear; while some adaptors bind more tightly, other

adaptors such as UBXD1 conversely lose binding to mutant p97, preferring instead to bind to the ADP-like down conformation (*58*, *121*, *123*). This question will be addressed more by functional assays in Chapter 4.

The rapid binding kinetics we observe with the p97-p47 and p97-UN complexes are in agreement with the rapid adaptor exchange we observed in cell lystate by MS, suggesting that some network regulation may come from rapid p97 sampling of adaptors. However, the fast off-rates of adaptors raises the question of how p97-adaptor complexes can properly function in the cell. The ATPase rate of p97 is between 0.75-5.2 ATP per second per hexamer (*28*, *32*, *95*, *118*), yet the off-rates of adaptors we measured ranged from 0.2-2 per second. In the slowest case, p97-UN would hydrolyze 3 to 25 ATP per hexamer during the lifetime of the complex, and in the extreme case of p47, at most 1 to 2 ATP would be hydrolyzed since p47 also retards p97 ATPase activity (*47*, *79*). Given these rates, it is unclear how p97 can engage substrate and sustain unfoldase activity without other mechanisms that modulate the lifetimes of these complexes. p97 and its adaptors are decorated with PTMs (*48*, *139*); for example, methylation of p97 at K315 has been proposed to affect its ATPase activity (*140*). Covalent modifications or interactions with other proteins, such as substrates, may serve to stabilize p97-adaptor complexes. Consistent with this hypothesis is the observation that p47 forms an extremely stable complex with p97 when purified from rat liver yet did not coelute with p97 in our SEC-MS experiments (*63*).

2.4 Methods

p97-p47 FRET reagents

Full-length p97 was amplified by PCR from human p97 pET15T (*28*) and ligated into pET24b using NdeI/SalI to produce a noncleavable C-terminal His-tagged construct. For FRET studies, p97 coding sequences were amplified by PCR and ligated into a modified pET28a vector to produce a construct with a noncleavable C-terminal His-tag and an N-terminal ybbR tag with a short linker (MDSLEFIASKLAGGGS). The construct for full-length p47 with a noncleavable N-terminal His-tag (*80*) was obtained through Addgene (#21268), and site-directed mutagenesis was used to make a p47-Thr370Cys mutation. Proteins were expressed and purified as described previously (*28*), with the exception that p47 was expressed in TOP10 cells for 3 h at 37 °C. For FRET, p47-Thr370Cys was incubated with tetramethylrhodamine-5-maleimide (ThermoFisher) prior to gel filtration to produce $p47^{TAMRA}$. For ybbR labeling, Cy5-CoA conjugate and Sfp enzyme were made as

described (*132*). Thirty micromolar ybbR-VCP was incubated for at least 3 h at room temperature with 60 μM Cy5-CoA conjugate and 12 μM Sfp in 50 mM HEPES pH 7.4, 10 mM $MgCl_2$ prior to gel filtration. All proteins were purified on a Superose 6 gel filtration column.

UN FRET reagents

An N-terminal sortase recognition motif was added to the N-terminus of Npl4 (*50*) to form MGGG-Npl4. To prevent labeling of His-Ufd1 (*125*), site directed mutagenesis was used to remove residue G2. This modified UN was expressed and purified as previously described (*141*) with one modification. Prior to gel filtration, 30 μM UN was labeled using 500 μM peptide (^{TRITC}WSHPQFEKLPETGG, GenScript) and 5 μM sortase (*135*) in labeling buffer (25 mM Hepes pH 7.4, 150 mM NaCl, 10 mM $CaCl_2$, 1 mM DTT) at 25 °C for 2 hours. The reaction was diluted in Strep-tag buffer (100 mM Tris pH 8.0, 150 mM NaCl, 1 mM EDTA) and incubated with 2 mL of Strep-Tactin resin (IBA Lifesciences) for 10 minutes at 4 °C with agitation. Resin was washed with 5 column volumes of Strep-tag buffer and eluted with Strep-tag buffer plus 50 mM biotin.

Mixed hexamer preparation

A plasmid for co-expression of p97 and p97-A232E-His was constructed via Gibson cloning to insert sequences from p97-His and p97-A232E-His into a pCOLA-Duet backbone. Protein was expressed in Rosetta DE3 overnight at 16 °C overnight with 0.4 mM IPTG. Cell pellet was resuspended in nickel binding buffer (50 mM Tris pH 7.4, 500 mM KCl, 5 mM $MgCl_2$, 20 mM imidazole, 5% glycerol, 2 mM β-mercaptoethanol) with protease inhibitors and sonicated. Clarified lysate was bound to a HisTrapHP (GE Healthcare) and eluted in a stepwise gradient of 12% (wash), 20% ('Mixed 1'), 35% ('Mixed 2'), and 55% ('Mixed 3') nickel binding buffer with 300 mM imidazole. Proteins were purified on a Superose 6 column (GE Healthcare) in storage buffer (20 mM Hepes pH 7.4, 250 mM KCl, 1 mM $MgCl_2$, 5% glycerol, 0.5 mM TCEP), concentrated, and flash frozen.

p97-p47 FRET measurements

All FRET measurements were carried out in 20 mM Hepes, pH 7.4, 100 mM KCl, 3 mM $MgCl_2$, 1 mM TCEP, and 1 mg/ml ovalbumin (Sigma). Nucleotides were optionally present at 2 mM, and inhibitors were optionally present at 15 μM. Equilibrium binding assays were carried out on a FluoroLog-3 (Jobin Yvon), with

excitation at 540 nm and emission scan 555–750 nm. Stopped-flow experiments were carried out on a Kintek SF-300X instrument with excitation at 540 nm and a 580/20 emission filter. Data were analyzed using Prism 6 (GraphPad).

p97-UN FRET measurements

Assays were carried out at room temperature in assay buffer (20 mM Hepes pH 7.4, 150 mM KCl, 20 mM $MgCl_2$, 1 mM TCEP, 1 mg/mL bovine serum albumin (BSA)) supplemented with 2mM ADP, 2 mM ATPγS, or ATP regeneration system (5 mM ATP, 30 mM creatine phosphate, 50 μg/mL creatine phosphokinase). Equilibrium binding assays were measured on a fluorometer (Photon Technology International, Inc) with 50 nM $U^{TRIRC}N$. Data were fit to a parabolic binding equation. Kinetic constants were measured using an AutoSF-120 stopped flow fluorimeter (KinTek) with an excitation wavelength of 540 nm and an emission filter of 576 ± 31 nm. For measurements of k_{on}, the final concentrations were 50 nM $U^{TRITC}N$ and 50-400 nM ^{Cy5}p97. Data were fit to single exponential decay equation to fit k_{obs}, and linear regression of k_{obs} versus [^{Cy5}p97] were used to calculate k_{on}. For measurements of k_{off}, 100 nM $U^{TRITC}N$ and 500 nM ^{Cy5}p97 were incubated before mixing with 5 μM UN (final dilution 2X). Data were fit to a single exponential association equation to extract k_{off}. For competition FRET experiments, final concentrations were 25 nM $U^{TRITC}N$, 25 nM ^{Cy5}p97-A232E, and various values of unlabeled p97 protein. Fluorescence intensity was measured on a Synergy Neo2 plate reader (BioTek) using a 540 nm excitation filter and 590 nm emission filter. FRET efficiencies were calculated from a control $U^{TRITC}N$ sample, and percent inhibition was calculated relative to a $U^{TRITC}N$-^{Cy5}p97-A232E sample. Inhibition curves were fit to an IC_{50} equation, and K_i was calculated using the known K_D of $U^{TRITC}N$-^{Cy5}p97-A232E and protein concentrations.

Protomer exchange assay

A plasmid encoding p97-FLAG for bacterial expression was made through the addition of a FLAG tag to a plasmid encoding untagged p97 in a pET24b backbone (RDB#3376). Protein was expressed in Rosetta DE3 as previously described (*141*). Harvested cells were resuspended in lysis buffer (50 mM Tris pH 7.4, 150 mM KCl, 5 mM $MgCl_2$, 5% glycerol) with protease inhibitors (Roche) and sonicated. Clarified lysate was incubated with 1 mL anti-FLAG resin (Sigma) at 4 °C for 1 hour. Resin was washed with 3 column volumes of wash buffer (50 mM Tris pH 7.4, 400 mM KCl, 5 mM $MgCl_2$, 0.5% Triton X-100) three times for ten minutes with rotation

followed by one wash with elution buffer without FLAG peptide (25 mM Hepes pH 7.4, 150 mM KCl, 2 mM $MgCl_2$). Protein was eluted with 2 mL of elution buffer containing 0.2 mg/mL 3XFLAG peptide for ten minutes with rotation. Elution was repeated, and resin was drained with a final 2 mL of elution buffer. After elution, concentrated protein was purified by gel filtration (Superose 6) in storage buffer (20 mM Hepes pH 7.4, 250 mM KCl, 1 mM $MgCl_2$, 5% glycerol, 0.5 mM TCEP) before flash freezing.

A solution of 250 nM of ^{Cy5}p97-His with or without 250 nM p97-FLAG was incubated for ten minutes at 25 °C with 25 μL anti-FLAG resin (Sigma) in 100 μL exchange buffer (50 mM Tris pH 7.4, 150 mM NaCl, 10 mM $MgCl_2$, 0.01% Triton X-100, ATP regeneration system). Resin was washed three times with 500 μL of exchange buffer without ATP regeneration system, and resin was boiled in SDS-PAGE sample buffer to elute. Samples were run on a 7% SDS-PAGE gel and imaged on a ChemiDoc (BioRad).

Chapter 3

IN VITRO RECONSTITUTION OF P97 UNFOLDASE ACTIVITY

The entirety of this chapter was originally published in: Blythe, E.E., Olson, K.C., Chau, V., Deshaies, R.J. (2017) Ubiquitin- and ATP-dependent unfoldase activity of p97/VCP • NPLOC4 • UFD1L is enhanced by a mutation that causes multisystem proteinopathy. *Proc. Natl. Acad. Sci. USA* **114**, E4380-E4388.

3.1 Introduction

The common mechanism that underlies all of p97's cellular jobs is presumed to be the extraction and unfolding of ubiquitylated proteins (*21*, *142*). The nature of the majority of known p97 substrates—unstable, scarce, modified by ubiquitin, and not readily divorced from their contexts—presents challenges for studying the enzymatic activity of p97 in a systematic manner. A major barrier to progress has been the absence of a simple, rapid, quantitative assay using defined components, that can be employed to dissect in detail the mechanism of action of p97. To address this obstacle, we have developed a soluble, monomeric p97 substrate. Our substrate is based on a non-cleavable ubiquitin fusion protein, Ub^{G76V}GFP, which is targeted for proteolysis by the Ub fusion degradation (UFD) pathway (*143*). Normally, ubiquitin fusions are co-translationally cleaved by a deubiquitinating enzyme to remove the ubiquitin (*144*). However, if the C-terminal glycine is mutated, processing is blocked and the fusion is rapidly degraded. Previous studies have demonstrated that the degradation of these non-cleavable Ub fusion proteins, including Ub^{G76V}GFP, is dependent upon p97•UN in human, *Drosophila*, and yeast cells (*34*, *98*, *143*, *145*). We show that p97 can unfold Ub^{G76V}GFP modified with a K48-linked polyUb chain and that this reaction is dependent upon the nature of the Ub chain, UN, and p97 ATPase activity in D2. Our system provides the first direct demonstration of a p97 unfoldase activity that depends on predicted physiological requirements and will be an invaluable tool for further study of p97 mechanism.

3.2 Results

Substrate and Assay Design.

We chose to pursue the UFD pathway substrate Ub^{G76V}GFP because it is rapidly degraded in a p97-dependent manner in yeast, *Drosophila*, and human cells

(*34*) and is a well-behaved protein whose folding state can be easily monitored by fluorescence. As p97 substrates are often polyubiquitylated, and p97•UN binds polyubiquitin (*33*), we reasoned that Ub^{G76V}GFP would need to be polyubiquitylated to be recognized. To efficiently ubiquitylate it, we developed a chimera of the RING domain from the E3 ubiquitin ligase gp78 and the E2 enzyme Ube2g2. Prior studies have shown that these enzymes catalyze formation of K48-linked ubiquitin chains (*33*). Notably, these two enzymes function upstream of p97 in ERAD, attesting to the physiological relevance of the use of these enzymes to generate a p97 substrate for our assay (*146*, *147*). Compared with Ube2g2 alone or unfused Ube2g2 with added gp78RING (Figure 3.1A), the gp78RING-Ube2g2 chimera produced unanchored polyubiquitin chains with very high efficiency (Figure 3.1B).

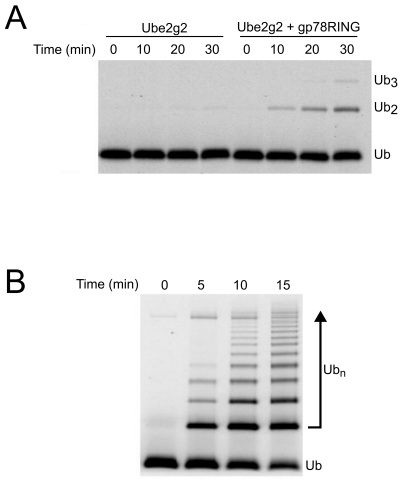

Figure 3.1: Characterization of gp78RING-Ube2g2 chimera. Time-courses comparing the rate of ubiquitin polymerization by 0.1 μM Ube2g2 alone or in the presence of 20 μM gp78RING (A), or when Ube2g2 is fused directly to gp78RING (B; assayed at 0.1 μM). The chimera is >6-fold faster than the unfused proteins.

Using this tool, we used various strategies to produce three types of potential p97 substrates. To simplify notation, linearly fused proteins are shown by dashes, and the length of the K48-linked ubiquitin chain attached to a particular ubiquitin is shown with a superscript preceding the initiator ubiquitin. First, we aimed to create a substrate with a short ubiquitin chain of defined length. Although the minimal requirement for recognition of ubiquitylated proteins by p97 is not known, the minimum ubiquitin chain length for recognition by the proteasome is four (*8*). Therefore, we enzymatically ligated Ub_3, in which the ubiquitins were joined via K48 linkages and the distal ubiquitin carried a K48R mutation, onto the linearly fused ubiquitin to form pure ^{Ub3}Ub-GFP (Figure 3.2A) (*148*, *149*). Second, to create a substrate with longer polyubiquitin chains, we built K48-linked chains directly onto the linearly fused ubiquitin (Figure 3.2B). Finally, to produce substrate with branched ubiquitin chains, we built ubiquitin chains on a

base substrate containing two or more linearly fused ubiquitins (Ub-Ub-GFP or Ub-Ub-Ub-GFP; Figure 3.2C). Heterogeneous substrates were fractionated by size-exclusion chromatography to enrich for different chain lengths (Figure 3.2D). One concern we had was the potential for GFP to refold after being processed by p97, leaving the assay without an observable endpoint. To address this, we added an ATPase mutant of the chaperonin GroEL. The GroEL D87K "trap" retains the ability to bind unfolded proteins but can no longer release those proteins (*150*). This dead-end complex sequesters unfolded GFP, preventing it from refolding, and has been used previously to provide assay endpoints for other unfolding machines (*88*).

GFP is unfolded by p97 in an Ub- and UN-dependent manner

To explore the unfolding potential of p97, we first compared a set of Ub-GFP substrates bearing K48-linked ubiquitin chains of varying lengths (Figure 3.4A). When mixed with p97, UN, and GroEL (Figure 3.2), Ub-GFP and ^{Ub3}Ub-GFP showed no appreciable loss of GFP fluorescence (Figure 3.4B). However, Ub-GFP with both "medium" (>4 Ub, ^{UbM}Ub-GFP) and "long" (>12 Ub, ^{UbL}Ub-GFP) ubiquitin chains showed a modest decrease in fluorescence over time (30%, Figure 3.4). Whereas ^{UbL}Ub-GFP did show improved unfolding relative to ^{UbM}Ub-GFP, the difference was quite small (5% signal loss).

We examined further the requirements for p97-dependent unfolding using ^{UbL}Ub-GFP, since this substrate gave the largest signal. When incubated with only p97 or p97 and GroEL, no unfolding was observed (Figure 3.4C). A similar result was obtained when UN was replaced with p47 or UBXD7, p97 adaptors involved in Golgi reassembly after mitosis (*63*) and regulation of cullin-RING Ub ligases (*49*, *60*, *151*), respectively, despite both of these adaptors binding to p97 and substrate (Figure 3.5). Therefore, UN is required for p97-catalyzed unfolding, and it cannot be replaced by other adaptors. Additionally, GroEL was essential to provide an endpoint for the assay. Fluorescence loss was amplified by the addition of GroEL (Figure 3.4C), indicating GFP was able to refold to some degree after processing by p97•UN. However, GroEL did not unfold substrate on its own (Figure 3.4C), and immunoprecipitation of GroEL showed that p97•UN was required for GroEL interaction with substrate (Figure 3.4D). Unfolding of substrate by p97 was also highly temperature dependent, with the rate and extent of unfolding increasing between 22-42 °C (Figure 3.6).

We found it curious that ≤40% of the fluorescence signal of ^{UbL}Ub-GFP was

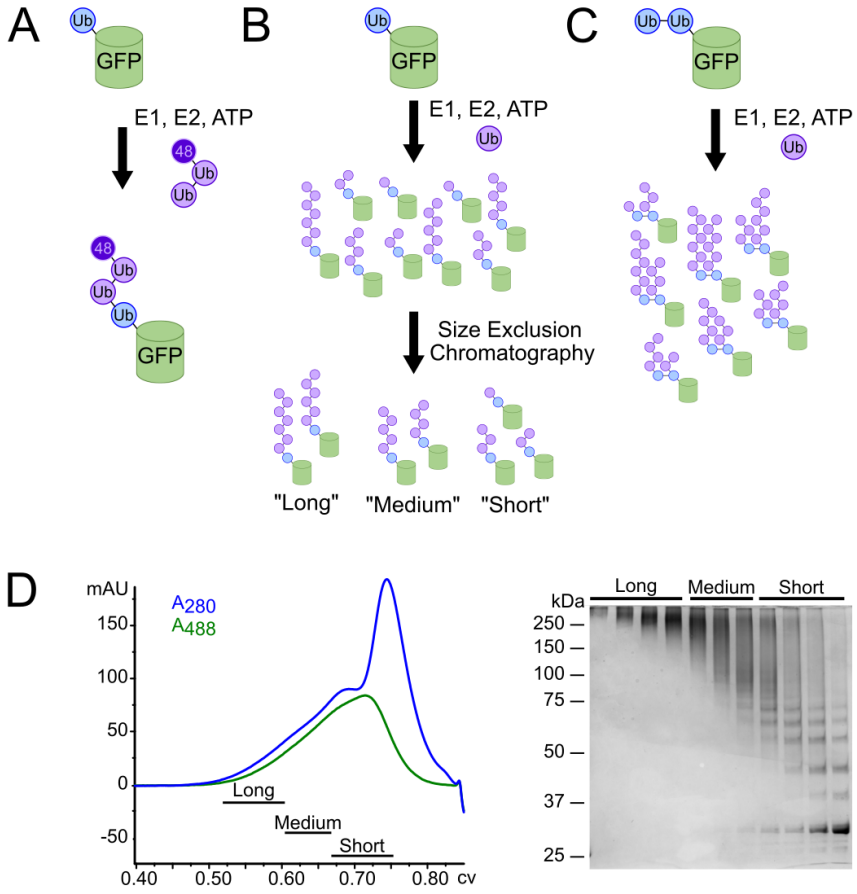

Figure 3.2: Substrate design and synthesis. (A) Preassembled, K48-linked Ub_3 chains containing a K48R mutation on the distal ubiquitin were ligated onto a noncleavable linear His_6-Ub-GFP fusion protein to produce pure ^{Ub3}Ub-GFP. (B) E1, E2, ubiquitin, and ATP were added to His_6-Ub-GFP to elongate K48-linked ubiquitin chains of varying lengths on the ubiquitin fused to GFP. These resulting substrates were purified from free ubiquitin chains via Ni-NTA resin and crudely fractionated according to chain length via size-exclusion chromatography to produce pools of "long-", "medium-", and "short"-chain substrates (^{UbL}Ub-GFP, ^{UbM}Ub-GFP, and ^{UbS}Ub-GFP, respectively). (C) To produce branched chains, ubiquitin chains of varying length were enzymatically elongated on a di- or triubiquitin linear fusion protein, Ub-Ub-GFP, or Ub-Ub-Ub-GFP, similar to B. (D) Size-exclusion chromatogram and corresponding SDS/PAGE gel for the purification of substrate described in B.

typically lost in our unfolding assays even though all components of the system were at or very near saturation (Figure 3.7), suggesting that there was another factor influencing substrate competence that remained to be discovered. Three Ub binding sites with different chain linkage preferences are available on p97•UN (*33*). Therefore, we tested whether substrates carrying branched Ub chains would be more effectively unfolded, because a branch would enable two separate ubiquitin chains to be elaborated from a single attachment point (in this case, Met1 of GFP). As a proxy for Ub chains with branched linkages, we expressed Ub-GFP fused to one or more

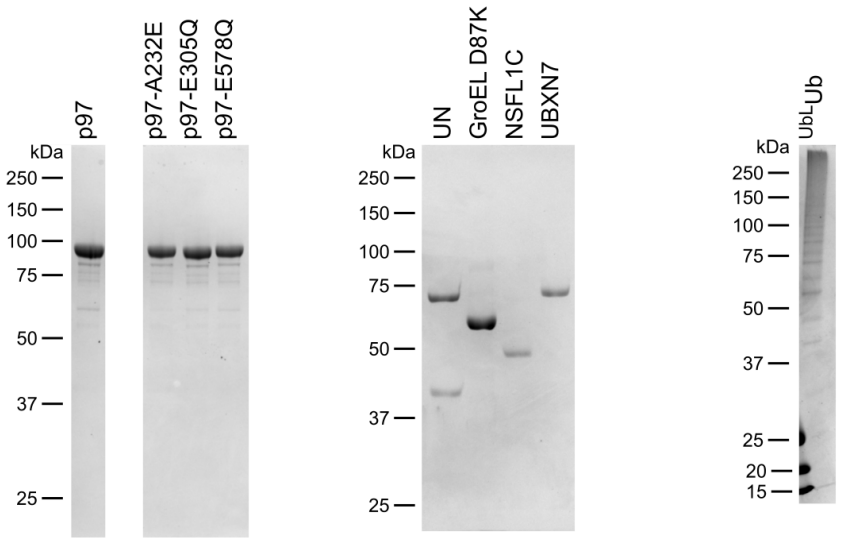

Figure 3.3: SDS-PAGE analysis of proteins used in this study.

additional ubiquitins in tandem and used these proteins as substrates for subsequent enzymatic polyubiquitylation (Figure 3.8A). Interestingly, a substrate in which K48-linked polyubiquitin chains were polymerized on Ub-Ub-GFP (^{UbM}Ub-^{UbM}Ub-GFP) showed significant improvement in unfolding by p97 as compared to ^{UbM}Ub-GFP (Figure 3.8B) despite the latter having a greater amount of ubiquitin conjugation as judged by mobility upon SDS-PAGE (Figure 3.8A, lanes 1 and 2). Neither further extension of the chains to form ^{UbL}Ub-^{UbL}Ub-GFP nor use of a triubiquitin fusion significantly increased the rate or extent of unfolding (Figure 3.8B). Although we cannot directly visualize ubiquitin chains branching from each ubiquitin in the Ub-Ub-GFP fusion protein, reactions run with Ub-K48R indicate that both Ub moieties were efficiently conjugated with ubiquitin under our reaction conditions (Figure 3.9). Incidentally, this same reaction confirms the linkage specificity of our Ube2g2–gp78 E2–E3 chimera. Taken together, our data suggest that the physical arrangement of the Ub chains is important for unfolding by p97•UN, with the enzyme preferring substrates with at least one branch point that enables nucleation of more than one chain of K48-linked ubiquitins.

Substrate unfolding is dependent upon ATP hydrolysis and stimulates p97 ATPase activity

Next we examined the energy-dependence of p97-catalyzed unfolding. ^{UbL}Ub-^{UbL}Ub-GFP was not unfolded by p97 in the absence of nucleotide, and ADP or the nonhydrolyzable ATP analog ATPγS could not substitute for ATP (Figure 3.10A).

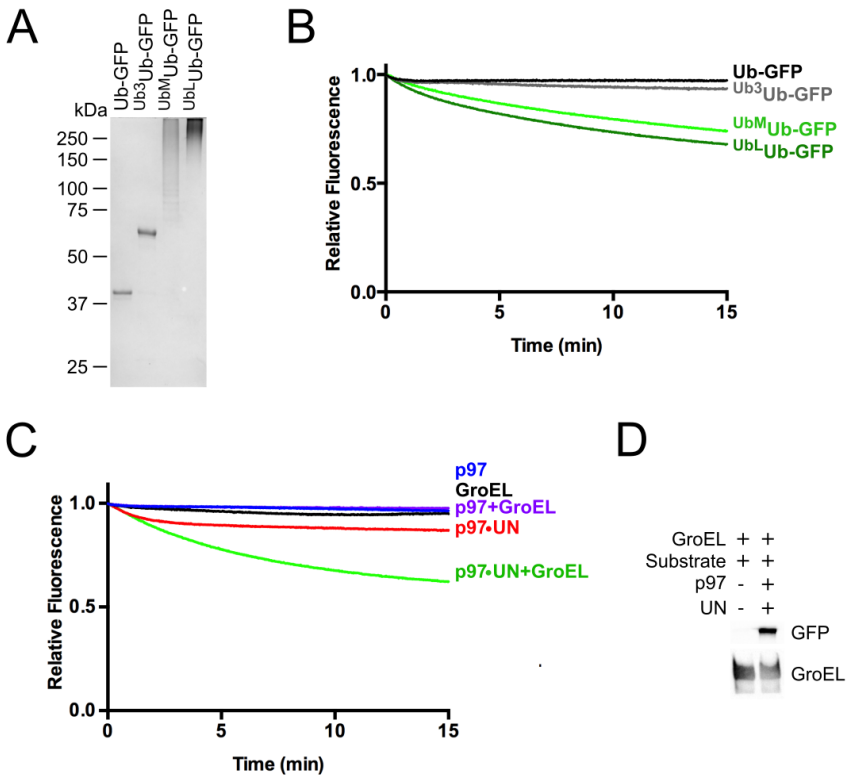

Figure 3.4: p97 unfolds Ub-GFP in a UN-dependent manner.(A) SDS/PAGE analysis of GFP substrates with different ubiquitin chain structures stained with Coomassie Brilliant Blue. (B) Upon addition of ATP, 75 nM p97, 150 nM UN, and 250 nM GroEL, 25 nM Ub-GFP, and ^{Ub3}-GFP did not appreciably lose fluorescence over time. However, Ub-GFP with "medium" or "long" K48-linked chains (^{UbM}Ub-GFP and ^{UbL}Ub-GFP) exhibited 26% and 32% loss of signal after 15 min, respectively. Representative traces shown (n ≥ 3). (C) Fluorescence of ^{UbL}Ub-GFP did not change over time with the addition of p97, GroEL, or p97 plus GroEL. Upon addition of p97 plus UN, a small decrease in signal was observed, and this decrease was augmented with the addition of GroEL. Representative traces shown (n ≥ 2). (D) ^{UbL}Ub-GFP coimmunoprecipitated with GroEL only in the presence of p97 and UN.

Two p97 ATPase inhibitors, the allosteric inhibitor NMS-873 (*14*) and the D2-specific, ATP-competitive inhibitor CB-5083 (*15*), also prevented ATP-dependent substrate processing (Figure 3.10A). p97 with a D1 domain Walker B motif mutation (p97-E305Q) that blocks nucleotide hydrolysis but not binding exhibited only mild defects in substrate unfolding. By contrast, the same mutation in D2 (p97-E578Q) completely abolished unfoldase activity (Figure 3.10B; Table 3.1). Together, these data demonstrate that ATP hydrolysis in D2 powers the unfolding of substrate by p97•UN.

Some adaptors modulate p97 ATPase activity (*79*), so we examined the effects of substrate processing on the hydrolysis of ATP by p97 and p97•UN. Addition of long unanchored K48-linked ubiquitin chains (^{UbL}Ub), Ub-GFP, ^{Ub3}Ub-GFP or ^{UbL}Ub-^{UbL}Ub-GFP did not alter the ATPase activity of p97 (Figure 3.11). Whereas

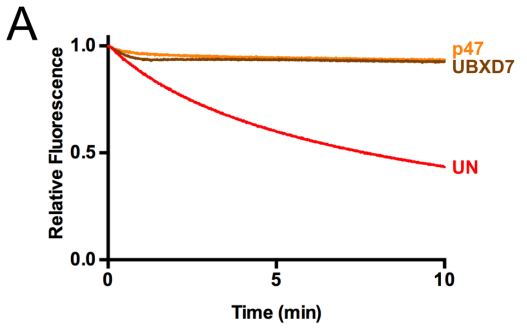

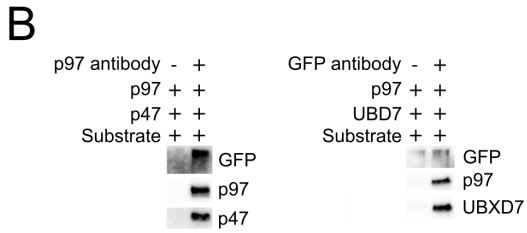

Figure 3.5: p97 adaptors p47 and UBXD7 do not promote substrate processing. (A) In the presence of p97 and GroEL, UN promoted a decrease in fluorescence of ^{UbL}Ub-^{UbL}Ub-GFP, indicating substrate unfolding. However, p47 and UBXD7 were not able to replace UN. Representative traces shown, n $\geq$ 2. (B) Both p47 and UBXD7 bind ^{UbL}Ub-^{UbL}Ub-GFP and mediate its interaction with p97, as shown by co-immunoprecipitation with purified proteins. Reactions contained 100 nM p97, 200 nM adaptor, and 200 nM substrate and were immunoprecipitated with antibodies to either GFP or p97, as indicated.

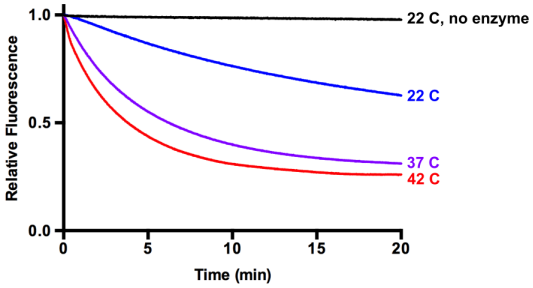

Figure 3.6: Unfolding by p97 is temperature dependent. Unfolding reactions using ^{UbL}Ub-^{UbL}Ub-GFP were carried out at 22 °C, 37 °C, and 42 °C. Higher temperatures increased both the rate and extent of the unfolding reaction. Representative traces shown, n $\geq$ 2.

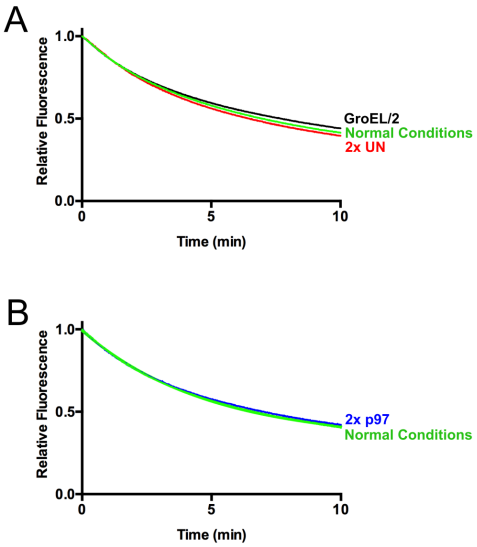

Figure 3.7: Unfolding reaction components are saturating. (A) When the concentration of GroEL was halved or the concentration of UN was doubled, minimal changes in the rate of unfolding of ^{UbL}Ub-^{UbL}Ub-GFP were observed. Representative traces shown, n = 2. (B) When the concentration of p97 was doubled, virtually no change in the rate of unfolding of ^{UbL}Ub-^{UbL}Ub-GFP was observed. Representative traces shown, n = 2.

UN did not significantly affect the ATPase activity of p97, the further addition of ^{UbL}Ub-^{UbL}Ub-GFP stimulated ATP hydrolysis by 4-fold, whereas Ub-GFP and ^{Ub3}Ub-GFP had no effect (Figure 3.10C). The latter result is consistent with the

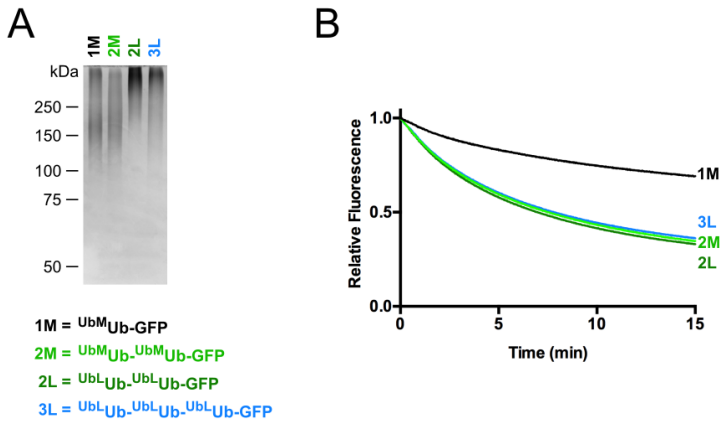

Figure 3.8: Branched ubiquitin chains are better p97 substrates. (A) SDS/PAGE analysis of Ub-GFP substrates stained with Coomassie Brilliant Blue. (B) Comparison of unfolding of substrates with one, two, or three ubiquitins fused in tandem to GFP. Note that substrate with two linearly fused ubiquitins (e.g., ^{UbM}Ub-^{UbM}Ub-GFP) was unfolded to a greater extent by p97 than substrate with a single linearly fused ubiquitin even though aggregate ubiquitination for the latter substrate was at least as extensive or greater than the former. Addition of an additional linearly fused ubiquitin (^{UbL}Ub-^{UbL}Ub-^{UbL}Ub–GFP) yielded no further improvement. Representative traces shown (n ≥ 3).

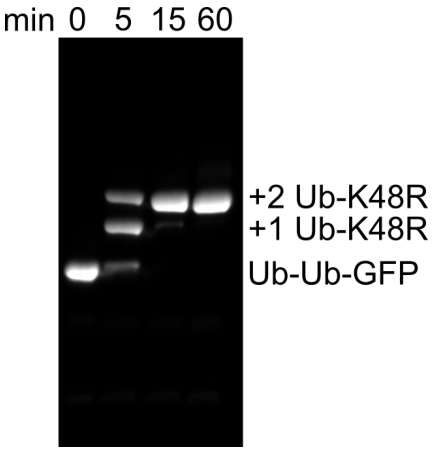

Figure 3.9: Two Ub-K48R can be added onto Ub-Ub-GFP. Time course of reaction of 10 μM Ub-Ub-GFP with 200 μM Ub-K48R under conditions identical to those used to make substrate produced pure ^{Ub1}Ub-^{Ub1}Ub-GFP, indicating that Ub chains are assembled on both fused ubiquitins in Ub-Ub-GFP. SDS-PAGE analysis of unboiled samples. GFP detected by excitation at 488 nm.

Mutant	Rate, min^{-1}	Plateau, %	n
WT	0.195 ± 0.007	33.3 ± 0.8	6
E305Q	0.154 ± 0.005	36.5 ± 0.8	3
E578Q	ND	ND	3
A232E	0.274 ± 0.007	25.3 ± 0.4	3

Table 3.1: Rates and extents of unfolding of ^{UbL}Ub-^{UbL}Ub-GFP by p97 mutants. The rates and plateaus were calculated by fitting data to a single exponential decay, with the plateau representing the percentage of fluorescence remaining at the end of the reaction. Unpaired t tests comparing WT rates vs. those of p97-E305Q and p97-A232E yielded P values of < 0.0001 in both cases, indicating statistically significant differences. Sample size represents number of technical replicates, and values are shown ± SD. ND, not detected.

inability of p97•UN to unfold Ub-GFP or ^{Ub3}Ub-GFP. Neither p47 nor UBXD7 supported substrate-triggered acceleration of p97 ATP hydrolysis (Figure 3.11B). Long, unanchored Ub chains also stimulated p97 ATPase activity to a similar degree

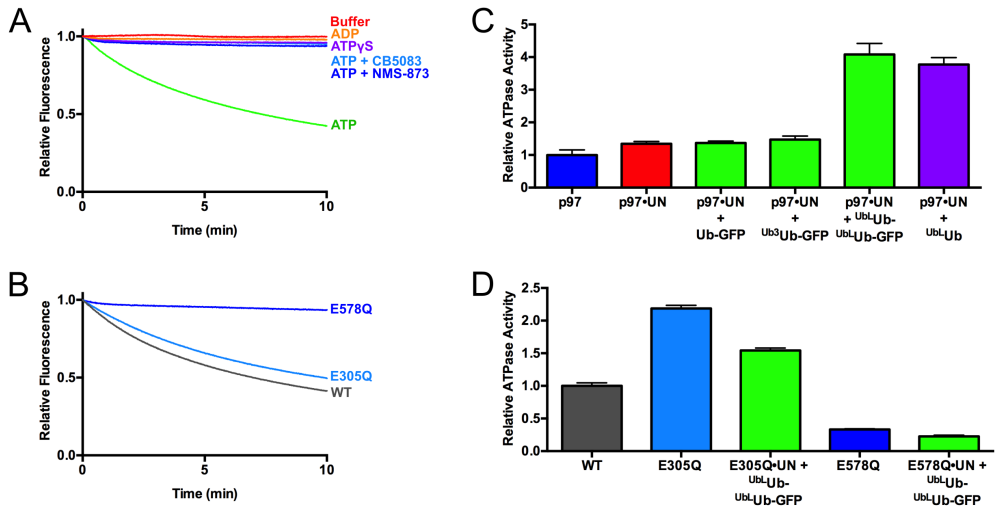

Figure 3.10: ATPase activity of p97 is critical for and stimulated by substrate unfolding. (A) Fluorescence traces of ^{UbL}Ub-^{UbL}Ub-GFP in the presence of p97, UN, GroEL, and various nucleotides and p97 inhibitors. Unfolding was observed only in the presence of ATP. Representative traces shown (n ≥ 2). (B) Unfolding of ^{UbL}Ub-^{UbL}Ub-GFP by p97 ATPase mutants. p97-E305Q and p97-E578Q are deficient in D1 and D2 ATPase activity, respectively. p97-E305Q was able to unfold substrate, whereas p97-E578Q was not. Representative traces shown (n ≥ 3). (C) Substrate stimulates ATPase activity of p97 when UN is present. Unanchored ubiquitin chains and those linked to Ub-GFP yielded equivalent stimulation, whereas Ub-GFP and ^{Ub3}Ub-GFP did not stimulate. ATPase activity was measured with BIOMOL Green as described in Methods and was normalized to basal WT p97 activity. Error bars represent SD (n = 4). (D) Effect of substrate plus UN on ATPase activity of D1 and D2 domain ATPase mutants. Addition of ^{UbL}Ub-^{UbL}Ub-GFP plus UN slightly decreased ATPase activities of D1 mutant E305Q and D2 mutant E578Q. Error bars represent SD (n = 4).

as ^{UbL}Ub-^{UbL}Ub-GFP, suggesting that p97 interaction with Ub chains and not the GFP substrate itself was both necessary and sufficient for the observed acceleration. In agreement with the unfolding results, the residual ATPase activity of p97-E578Q was unaffected by substrate plus UN (Figure 3.10D). However, p97-E305Q, which was able to unfold substrate, was also not stimulated by substrate, even showing a slight decrease in ATPase activity (Figure 3.10D). The E305Q mutant also showed higher basal ATPase activity than WT, as has been seen before in steady-state experiments (*28*). These results suggest that there is a high degree of crosstalk between ATPase activity in D1 and D2, and whereas ATP hydrolysis in D2 is the driving force for unfolding, D1 activity is also needed for substrate-induced ATPase acceleration.

UN recruits substrate to p97

The tight correlation between the competence of a substrate to be unfolded and its ability to accelerate ATP hydrolysis suggests that binding of substrate to p97 may stimulate ATPase activity, leading to substrate unfolding. To further probe this hypothesis, we evaluated binding of substrate to p97. Immunoprecipitation of p97

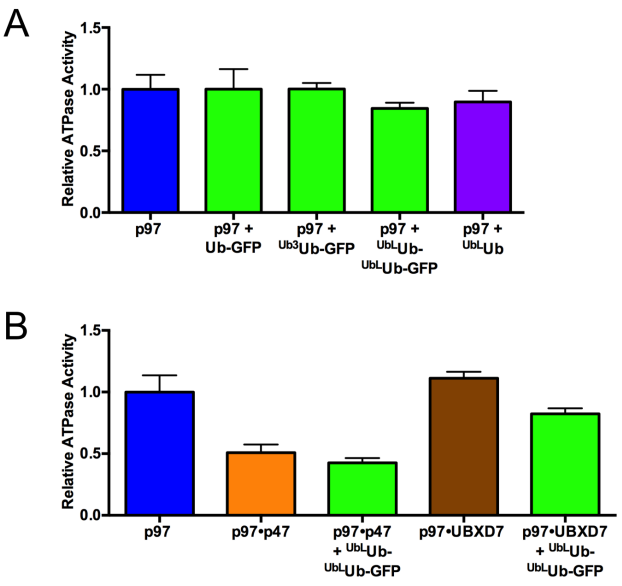

Figure 3.11: Substrate alone or in complex with other adaptors does not accelerate p97 ATPase. (A) ATPase activity of p97 is not affected by substrate when UN is absent. (B) p47 and UBXD7 do not promote substrate-induced ATPase acceleration. Addition of substrate did not significantly change the ATPase activity of p97•p47 or p97•UBXD7. ATPase activity was measured with BioMol Green as described in Methods. Error bars represent S.D. with n = 4.

showed that it bound ^{UbL}Ub-^{UbL}Ub-GFP substrate in the presence but not in the absence of UN (Figure 3.12, lanes 4 and 5). Reciprocal immunoprecipitation of GFP confirmed that substrate bound UN in the absence of p97 but did not bind p97 in the absence of UN (Figure 3.12). Furthermore, the interaction between p97 and UN appeared to be stabilized by substrate binding (Figure 3.12, lanes 3 and 5). We also analyzed substrate dependence of GroEL association with p97, but observed high background binding to our beads even in the absence of antibody (lane 1). The binding signal was increased in lanes 6 and 7, but this could be due to p97, which in our experience is prone to exhibit non-specific binding.

Whereas the unfolding of substrate was highly dependent on ATP hydrolysis, substrate interaction with p97 was not. Immunoprecipitation of $^{FLAG\text{-}UbL}$Ub-$^{FLAG\text{-}UbL}$Ub-GFP pulled down equal amounts of p97 in the absence of added nucleotide and in the presence of ATP, ATPγS, ATP plus NMS-873, and ATP plus CB-5083 (Figure 3.12). Therefore, p97 does not have to be actively remodeling substrate in order to effectively form a tight complex. Loss of binding of p97, but not UN, was seen only with added ADP, which could be due to the large conformational changes observed for p97 in its ADP-bound state (*22*) (Figure 3.12). These results are consistent with previous studies on Ub chain association with p97 and p97•UN (*52*, *152*).

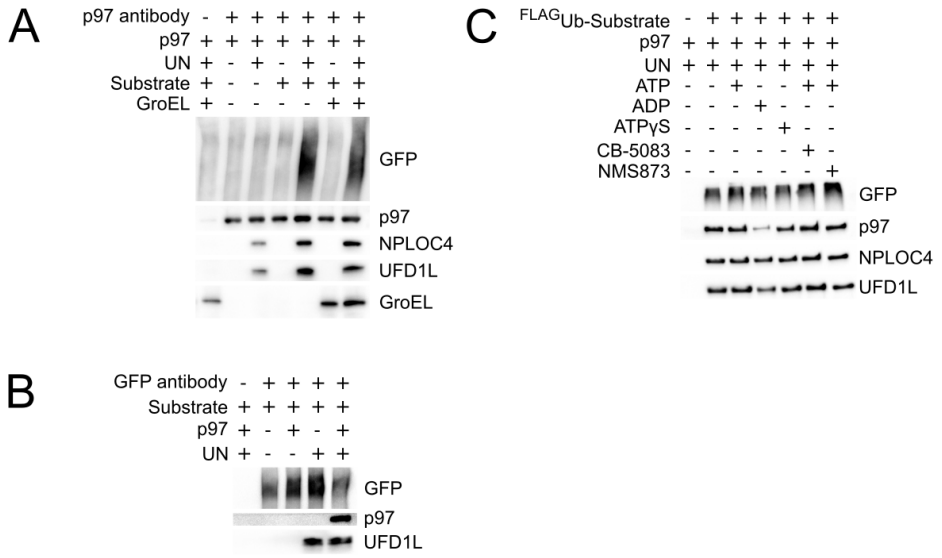

Figure 3.12: UN recruits ubiquitylated substrate to p97. (A) Association of substrate with p97 depends on UN. Reactions containing 100 nM p97, 200 nM UN, 200 nM ^{UbL}Ub-^{UbL}Ub-GFP and/or 200 nM GroEL were immunoprecipitated using an anti-p97 antibody and assessed by western blot. Substrate was pulled down with p97 only in the presence of UN, and substrate enhanced the binding of UN to p97. Effects of substrate and UN on binding of GroEL to p97 could not be determined due to high background binding of GroEL to beads, antibody and/or p97. (B) UN binds directly to substrate and links it to p97. Samples prepared as in (A) were immunoprecipitated with an anti-GFP antibody. Substrate pulled down UN but only bound p97 in the presence of UN. (C) Bound nucleotide has only a modest effect on formation of a p97•UN•substrate ternary complex. Samples prepared as in (A) with various nucleotides and/or p97 inhibitors were immunoprecipitated by anti-FLAG resin, which bound the FLAG-tagged Ub on substrate. Binding of p97, but not UN, was reduced only in the ADP state.

3.3 Discussion

P97/VCP is implicated in a broad range of cellular processes including membrane fusion, protein trafficking, and ubiquitin dependent proteolysis (*27*). It is thought that the core biochemical activity of p97 that enables its diverse biological functions is its ability to act as a segregase that segregates polypeptides from binding partners in multisubunit complexes, or from large macromolecular structures including ribosomes, membranes, or chromatin. Although the mechanism by which p97 exerts segregase activity is not known, the most economical hypothesis is that it grabs onto the polypeptide to be segregated and commences to unfold it. However, despite the appeal of this unifying hypothesis, the ability of WT p97 to harvest the energy of ATP hydrolysis to unfold a polypeptide has never been directly demonstrated. We show here, in a well-defined system, that WT p97 can at least partially unfold a protein. In contrast to prior studies that used a doubly mutated p97 acting upon an unmodified protein in the absence of any adaptor (*153*, *154*), the unfolding we observe exhibits dependencies predicted from prior genetic and biochemical studies of p97, including dependence on ATP hydrolysis by the D2 AT-

Pase domain of p97, the heterodimeric adaptor NPLOC4•UFD1L, and conjugation of an ubiquitin chain to the substrate that is unfolded (*27*, *32*, *33*).

Despite the close alignment of in vitro dependencies reported here with known in vivo requirements for p97 action, there are two caveats worth noting. First, we do not know whether the loss of GFP fluorescence is the result of complete unfolding or local unfolding. Second, our Ub-GFP model substrate is not a native substrate of p97. However, p97 activity in the UFD pathway is absolutely required for its degradation in vivo in yeast, *Drosophila*, and human cells (*34*, *98*, *143*, *145*), and the E2–E3 chimera used to ubiquitylate Ub-GFP was derived from enzymes that function directly upstream of p97 in the ERAD pathway (*146*). Thus, we believe the reaction reported here represents the essence of p97's biochemical activity that underlies its physiological functions.

Processing of our Ub-GFP substrate by p97 is dependent on the conjugation of multiple ubiquitins connected by K48 linkages, which is consistent with reports of K48-linked ubiquitin chain binding by p97 and UFD1L and linkage-nonspecific chain binding by NPLOC4 (*33*, *52*, *77*, *152*). One of our most interesting findings is that we observed enhanced substrate unfolding when the substrate contained a branch point enabling the formation of multiple K48-linked ubiquitin chains. Our substrate contains a branch at the base of the ubiquitin conjugate, which allows for two K48-linked chains to be built on a single site of substrate modification. Because there are multiple ubiquitin binding sites on the p97•UN complex, the branched chain on our ^{UbL}Ub-^{UbL}Ub-GFP substrate may retard, via enhanced avidity, its dissociation before unfolding. Branched ubiquitin chains can enhance substrate degradation (*102*) and have been associated with p97 previously. Ubiquitin chains with K11 linkages are associated with multiple p97 adaptor proteins (*49*) and are implicated in ERAD (*155*). Substrates modified with K11 and K11–K48 branched chains associate with p97•UN and its *Drosophila* ortholog (*134*, *156*), and p97 binds K11–K48 branched chains better than either type of homotypic chain (*102*). Furthermore, K29 and K48 linkages are formed on UFD pathway substrates in vivo and in vitro using purified UFD pathway enzymes (*98*, *101*). Whereas our data with linear ubiquitin fusions suggest that branched and/or multiple ubiquitin chains may be important for interaction of substrates with p97•UN, further work with physiological linkages in vitro and in vivo is needed to determine the exact requirements for ubquitylated p97 substrates.

The second requirement for p97-catalyzed unfolding is the heterodimeric

adaptor UN. In agreement with prior work, UN bridges the interaction of substrates with p97 (*33*, *52*). However, p97 also associates with other adaptor proteins, some of which (e.g., UBXD7) can cobind with UN and others (e.g., p47) of which bind in a mutually exclusive manner (*49*, *51*, *65*, *66*, *71*). Although there are examples of processes that require UN and an additional adaptor (*59*, *157*), in general, it is unclear whether the different adaptors work in different pathways, or work sequentially, together, or in opposition to one another in the same pathway. Mutually exclusive adaptors like p47 bind very differently from UN yet also promote protein segregation (*63*, *76*, *78*). However, neither p47 nor UBXD7 was able to replace UN in our unfolding assay, suggesting they promote substrate processing in a different way or work on different substrates. Our assay provides the first platform for further mechanistic exploration of the functional relationship between different adaptor proteins.

The final requirement for unfolding of GFP is ATP hydrolysis by the D2 ATPase of p97. Our results are in direct contrast with a previous study which showed that p97-dependent unfolding is inhibited by ATP (*158*), but are consistent with overwhelming in vitro and in vivo data (*27*, *33*, *35*, *95*). Our experiments with p97 mutants and the D2-specific ATP-competitive inhibitor CB-5083 demonstrate the importance of D2 ATPase activity over that of D1, which confirms prior observations (*28–30*, *32–35*). We observed very little effect of the D1 Walker B mutant on substrate processing, leaving the role of D1 ATPase activity in p97 function unclear (*27*). Not only is the ATPase activity key to substrate processing but we also observe its stimulation by Ub chain or substrate binding. This stimulation was abolished in the D1 Walker B mutant. Nevertheless, this mutant unfolded GFP at near-WT rates, suggesting that substrate stimulation of ATP hydrolysis might not be essential, at least for some substrates. ATPase acceleration in the presence of the cytoplasmic fragment of the ERAD substrate Sytl has been previously reported, but unlike the stimulation reported here, it was not dependent upon UN or ubiquitylation of the substrate (*95*), both of which are thought to be requirements for ERAD. p97 can interact both with a substrate and the Ub chain appended to the substrate (*33*, *159*), suggesting that stimulation of p97 ATPase and perhaps substrate processing can be regulated through multiple binding interfaces.

3.4 Methods

Protein and expression purification

A description of the construction, expression and purification of novel reagents is described below. A description of previously published proteins used in this study can be found in Table 3.2.

RDB Number	Plasmid name	Vector	Expression	Purification	Comments	Ref.
3019	Ube1	pET28b	BL21, 0.5 mM IPTG, 16 °C for 16 hours	Ni-NTA, S200		(*160*)
2804	Cdc34	pGEX-6P-1	BL21, 0.4 mM IPTG, 25 °C for 16 hours	Glutathione sepharose, S200		(*148*)
3166	gp78-Ube2g2	pET28a	BL21, 0.4 mM IPTG, 25 °C for 16 hours	Ni-NTA, S75, TEV cleavage, MonoQ		This study
2805	His-Ub	pET15b	BL21, 0.4 mM IPTG, 16 °C for 16 hours	Ni-NTA, thrombin cleavage, S75		(*148*)
3348	His-Ub-K48R	pET15b	BL21, 0.4 mM IPTG, 16 °C for 16 hours	Ni-NTA, thrombin cleavage, S75		This study
3006	His-Ub-G76V-GFP	pET28a	BL21, 0.4 mM IPTG, 37 °C for 4 hours	Ni-NTA, S200		This study
3344	His-Ub2-G76V-GFP	pET28a	BL21, 0.4 mM IPTG, 37 °C for 4 hours	Ni-NTA, S200		This study
3345	His-Ub3-G76V-GFP	pET28a	BL21, 0.4 mM IPTG, 37 °C for 4 hours	Ni-NTA, S200		This study
3219	p97-His	pET24b	Rosetta, 0.1 mM IPTG, 25 °C for 16 hours	Ni-NTA, S6		(*87*)
3346	p97-His E305Q	pET24b	Rosetta, 0.1 mM IPTG, 25 °C for 16 hours	Ni-NTA, S6		This study
3347	p97-His E578Q	pET24b	Rosetta, 0.1 mM IPTG, 25 °C for 16 hours	Ni-NTA, S6		This study
3352	p97-His A232E	pET24b	Rosetta, 0.1 mM IPTG, 25 °C for 16 hours	Ni-NTA, S6		This study
2686	NPLOC4	pCOLA-Duet	BL21, 0.4 mM IPTG, 16 °C for 16 hours	Ni-NTA, S200	Co-purified with UFD1L	(*50*)
2796	His-UFD1L	pET28a	BL21, 0.4 mM IPTG, 16 °C for 16 hours	Ni-NTA, S200	Co-purified with NPLOC4	(*125*)
2886	His-p47	pTrcHis	TOP10, 0.4 mM IPTG, 37 °C for 4 hours	Ni-NTA, S200		(*80*)
2598	GST-FLAG-UBXD7	pGEX-4T-2-TEV	Rosetta, 0.4 mM IPTG, 37 °C for 4 hours	Glutathione sepharose, TEV cleavage, S200		(*60*)
3218	GroEL D87K	T7	TOP10 0.4 mM IPTG, 37 °C for 4 hours	HiTrap Q FF, S6, Affigel Blue		(*150*)

Table 3.2: Proteins used in this study.

gp78RING-Ube2g2 chimera construction and purification

A 72-residue sequence of the E3 ubiquitin protein ligase gp78/AMFR (residues 322 to 393), containing the RING domain, was fused to the N-terminus of the ubiquitin-conjugating enzyme Ube2g2 with a linker sequence of GTGSH. cDNA encoding this fusion protein was inserted into the bacterial expression plasmid

p28a-TEV vector to encode a polyHis-tagged protein. Protein was expressed in BL21(DE3) at 37 °C with 0.4 mM IPTG for 4 hours and was purified on Ni-NTA resin and a Superdex 75 column before being cleaved with TEV protease overnight at 4 °C. Cleaved protein was then bound to a MonoQ ion exchange column, eluted with a NaCl gradient (0.05 – 0.5 M), concentrated with centrifugal filter units, and flash frozen.

Ub^{G76V}GFP fusion construction

The coding sequence for Ub^{G76V}GFP in the EGFP-N1 vector (RDB# 1832) (*34*) was PCR amplified and inserted into pET28a using NdeI and NotI sites to produce His_6-Ub^{G76V}-GFP (RDB# 3006). His_6-Ub^{G76V}- Ub^{G76V}-GFP (RDB# 3344) and His_6-Ub^{G76V}-Ub^{G76V}-Ub^{G76V}-GFP (RDB# 3345) were created by ligating $Ub_2{}^{G76V}$ and $Ub_3{}^{G76V}$, PCR amplified from a synthetic $Ub_4{}^{G76V}$ sequence (RDB# 2406), into His-Ub^{G76V}-GFP cut with NdeI and HindIII. For simplification, the G76V notation has been left out of subsequent mentions of these constructs.

^{Ub3}Ub-GFP synthesis and purification

A plasmid for bacterial expression of Ub-K48R (RDB# 3348) was made from that of Ub (RDB# 2805) by site-directed mutagenesis, and the protein was expressed as previously described (*148*). Pure K48-linked Ub_3 chains carrying a K48R mutation in the distal Ub were enzymatically synthesized and purified as described previously (*148*, *149*). To form ^{Ub3}Ub-GFP, 0.5 μM Ube1 (E1), 5 μM gp78RING-Ube2g2, 2.5 μM Ub-GFP, and 5 μM Ub_3 were incubated in 20 mM Hepes pH 7.4, 5 mM ATP, and 5 mM $MgCl_2$ overnight at 37 °C. The ^{Ub3}Ub-GFP was then purified on Ni-NTA resin and a Superdex 200 gel filtration column before being concentrated with centrifugal filter units and flash frozen.

Polyubiquitylated substrate synthesis and purification

Reactions were carried out with final concentrations of 10 μM Ub-GFP fusion protein, 1 μM E1, 20 μM gp78RING-Ube2g2, and 400 μM ubiquitin in 20 mM Hepes pH 7.4, 10 mM ATP, and 10 mM $MgCl_2$ at 37 °C overnight. Ubiquitin was added progressively in small amounts over the first eight hours of the reaction. For FLAG-tagged substrate, 40 μM FLAG-Ubiquitin (Boston Biochem, Cambridge, MA, USA) was added in the first two hours. To purify ubiquitylated GFP from free ubiquitin chains, the reaction mixture was incubated with Ni-NTA resin, eluted with 300 mM imidazole, and run over a Superose 6 size exclusion column in 20 mM

Hepes, pH 7.4, 250 mM KCl, 1 mM $MgCl_2$, 1 mM TCEP and 5% glycerol. Fractions were pooled into long, medium, and short chain length samples, concentrated with centrifugal filter units, and flash frozen.

ATPase assays

The ATPase assay protocol was modified from previously published methods (*47*). In an untreated microplate (#655101, Greiner Bio-One, Kremsmünster, Austria), 40 μL solutions containing 30 nM p97 hexamer, 150 nM adaptor, and/or 150 nM substrate in ATPase assay buffer (25 mM Hepes pH 7.4, 100 mM KCl, 3 mM $MgCl_2$, 1 mM TCEP, 0.1 mg/mL ovalbumin) were preincubated at 37 °C for 10 minutes. To this, 10 μL of a 1 mM ATP solution was added, and the reaction was incubated at 37 °C for 5 or 10 minutes. After cooling on ice for 30 seconds, 50 μL of BIOMOL Green reagent (Enzo Life Sciences, Farmingdale, NY, USA) was added. Solutions were developed at room temperature for 30 minutes before being read at 600 nm. The amount of inorganic phosphate in each sample was calculated from a standard curve, and relative ATPase activity for a sample was calculated by normalizing its measurement to that of samples of WT p97 alone.

Fluorescence unfolding assays

Unless specified, all assays were carried out at 37 °C. Samples contained 25 nM GFP substrate, 75 nM p97 hexamer, 150 nM adaptor (UN, p47 or UBXD7), and/or 250 nM GroEL trap in unfolding assay buffer (25 mM Hepes pH 7.4, 100 mM KCl, 5 mM $MgCl_2$, 1 mM TCEP, 2 mM ATP). Control experiments indicated that the levels of p97, adaptor, and GroEL used were at or near saturation (Figure 3.7). Other nucleotides and p97 inhibitors were present at 2 mM and 10 μM, respectively, when indicated. Kinetic experiments were carried out on a Fluoro-Log 3 (Horiba Jobin Yvon, Edison, NJ, USA) with excitation at 488 nm and emission at 509 nm. Relative fluorescence was calculated by normalizing the fluorescence signal to that at time zero. Unfolding rates were calculated by fitting curves to an exponential decay model in Prism (GraphPad, San Diego, CA, USA).

Binding assays

Antibodies used for immunoprecipitation and western blotting are listed in Table 3.3. Samples containing 100 nM p97, 200 nM UN, 200 nM GFP substrate, and/or 200 nM GroEL trap in binding assay buffer (25 mM Hepes pH 7.4, 100 mM KCl, 3 mM $MgCl_2$, 1 mM TCEP) in a volume of 200 μL were preincubated at 37 °C

for 15 minutes. Triton X-100 interfered with binding of substrate to GroEL trap, so 0.01% Triton X-100 was included in all buffers only in reactions that did not contain GroEL. Nucleotides and inhibitors were present at 2 mM and 10 μM, respectively, where indicated. For IPs using Protein G magnetic beads (Bio-Rad Laboratories, Hercules, CA, USA), protein mixtures were incubated with 1 μL of antibody for 15 minutes at 37 °C prior to a 1 hour incubation with 25 μL of beads at room temperature. For FLAG IPs, reactions were incubated with 25 μL of anti-FLAG resin (Sigma-Aldrich, St. Louis, MO, USA) for 15 minutes at room temperature. Following incubation, all beads were washed 3 times with 750 μL assay buffer before being boiled in 50 μL 2X SDS-PAGE loading dye. Samples were then analyzed by western blot.

Purpose	Antigen	Source	Species	WB Titer
IP	p97	ab11433, Abcam, Cambridge, UK	mouse	NA
IP	GroEL	gift from Arthur Horwich	rabbit	NA
IP	GFP	ab290, Abcam, Cambridge, UK	rabbit	NA
IP	GFP	Living Colors JL-8, Clontech Laboratories, Inc, Mountain View, CA, USA	mouse	NA
WB	p97	ab11433, Abcam, Cambridge, UK	mouse	1 : 2000
WB	p97	H-120, Santa Cruz Biotechnology, Dallas, TX, USA	rabbit	1 : 2000
WB	UFD1L	611642, BD Biosciences, San Jose, CA, USA	rabbit	1 : 500
WB	UFD1L	13789, Cell Signaling Technologies, Danvers, MA USA	mouse	1 : 1000
WB	NPLOC4	13489, Cell Signaling Technologies, Danvers, MA USA	mouse	1 : 1000
WB	p47	sc134945, Santa Cruz Biotechnology, Dallas, TX, USA	rabbit	1 : 200
WB	UBXD7	AB10037, EMD Milliport, Billerica, MA, USA	rabbit	1 : 1000
WB	GFP	Living Colors JL-8, Clontech Laboratories, Inc, Mountain View, CA, USA	mouse	1 : 500
WB	GFP	ab290, Abcam, Cambridge, UK	rabbit	1 : 1000
WB	GroEL	82592, Abcam, Cambridge, UK	mouse	1 : 1000
WB, HRP conjugate	rabbit IgG	170-6515, Bio-Rad Laboratories, Hercules, CA, USA	goat	1 : 10 000
WB, HRP conjugate	mouse IgG	115-055-174, Jackson ImmunoResearch, West Grove, PA, USA	goat	1 : 10 000

Table 3.3: Antibodies used in this study.

Chapter 4

P97 MSP MUTANTS ARE BETTER UNFOLDASES

4.1 Introduction

With an in vitro assay of p97 unfoldase activity in hand, we were interested in directly assessing the effects of MSP mutants on this basic biochemical function of p97 for the first time. Such an assay gives us the ability to begin to distinguish between gain and loss of function models for MSP pathology. In our publication discussed in the previous chapter, we began to address this by testing a single MSP mutation, A232E, which is reported to have the most severe clinical MSP presentation (*81*). Under single turnover conditions, A232E showed accelerated unfolding compared to WT, indicative of a true gain of function (*141*). Importantly, this unfoldase activity could be restored to WT-like levels using a low dose of p97 inhibitor CB-5083, providing initial evidence that p97 inhibitors might be effective treatments for MSP (*141*).

To generalize our previous observations with A232E and further characterize this accelerated unfoldase activity in MSP mutants, we expanded our analysis to six additional MSP mutations, all of which showed moderately faster unfolding. We also characterize the unfoldase activities of mixed WT and A232E hexamers for the first time, disproving the hypothesis that mutant protomers can "poison" WT hexamers. By examining ATPase rates during substrate processing in pure mutant and mixed WT-mutant hexamers, we reveal that ATPase rates do not correlate with unfoldase rates. Instead, we propose that the differential UN, and therefore substrate, binding between WT and mutant hexamers described in Chapter 2 leads to the accelerated unfoldase rates we observe. Taken together, our data lends further support for the gain of function model for MSP pathology we previously proposed.

4.2 Results

Assay development

Our previous work employed a GFP-based substrate to demonstrate p97 unfoldase activity; however, that this assay's endpoint was dependent upon a mutant GroEL "trap" to bind unfolded protein was a limitation (*141*). In order to improve our assay, we redesigned our substrate, swapping in mEos3.2 for GFP (Figure 4.1A). Upon exposure to UV light, mEos3.2 undergoes a backbone cleavage, forming two

separate polypeptides and inducing a green-to-red fluorescence shift (*161*, *162*). This cleavage prevents protein refolding without the requirement for a GroEL "trap," and consequently others have employed mEos3.2 for studying p97 and its homologue Cdc48 (*163–165*). As before, we modified a linear fusion of di-ubiquitin-mEos3.2 with long K48-linked ubiquitin chains for recognition by UN, allowing it to be unfolded by p97-UN (*141*).

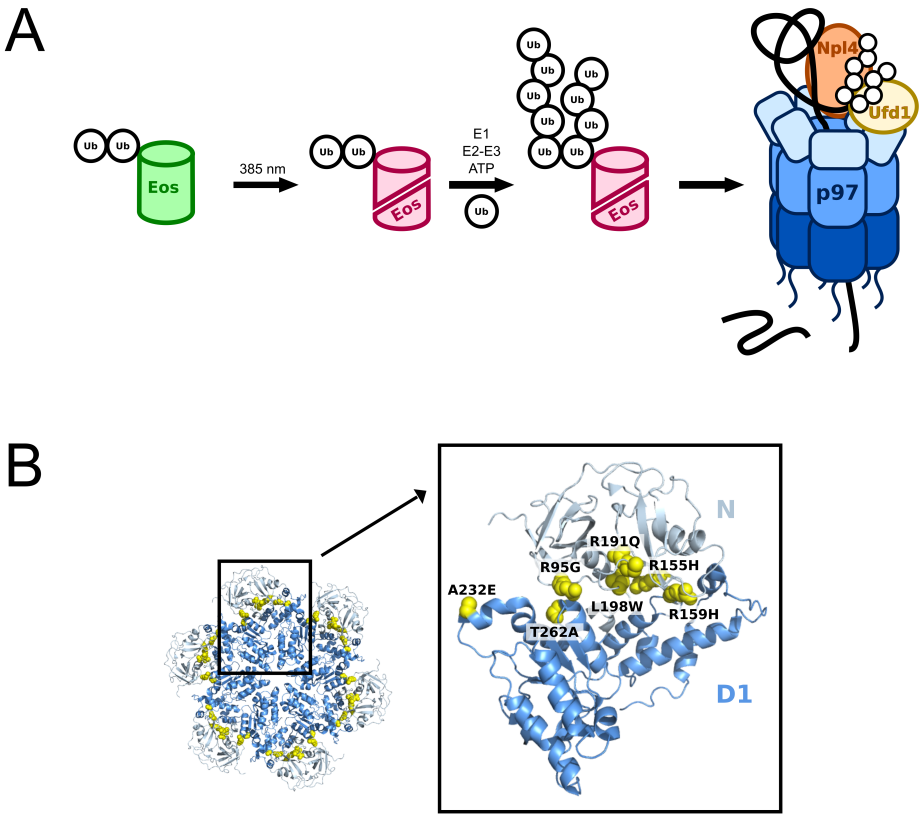

Figure 4.1: MSP unfoldase assay design. (A) Substrate design and unfoldase assay scheme. A linear fusion of di-ubiquitin and mEos3.2 is irradiated with UV light, causing a backbone cleavage and fluorescence shift in mEos3.2. Long, heterogeneous K48-linked ubiquitin chains are then built onto the substrate ubiquitins. Unfolding of the substrate by p97-UN can be observed by the loss of fluorescence since the two polypeptides of mEos3.2 cannot reassociate after processing. (B) MSP mutations used in this study. PDB #5FTK.

IBMPFD mutants have moderately enchanced unfoldase activities

In order to determine if faster unfolding of a model substrate is a definitive characteristic of MSP mutations, we used our updated substrate to assess the unfoldase activity of a total of seven MSP mutations, the locations of which on the N-D1 interface are shown in Figure 4.1B. Under single turnover conditions, all MSP mutants tested had accelerated unfoldase rates, ranging from approximately 115-160% of WT rates (Figure 4.2A-B, 4.3). This enhancement of activity was seen across three independent preparations of proteins, though variability was high

among different preparations of the mutant p97 proteins (Figure 4.4).

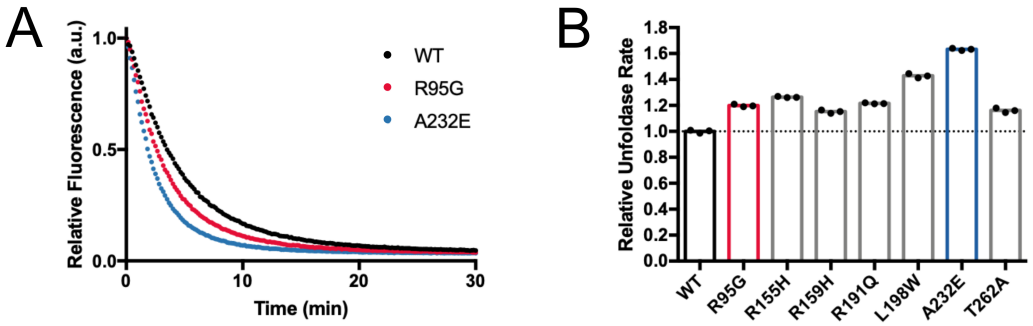

Figure 4.2: MSP mutants have moderately accelerated unfoldase rates. (A) Example unfoldase assay data showing a loss of mEos3.2 fluorescence over time. Experiment was run under single-turnover conditions with 20 nM substrate, 400 nM p97 hexamer, and 800 nM UN. (B) Unfoldase data across a panel of seven MSP mutations. Fluorescence data was fit to a single exponential, and rates were normalized to that of WT. Technical replicates shown with a bar representing the average.

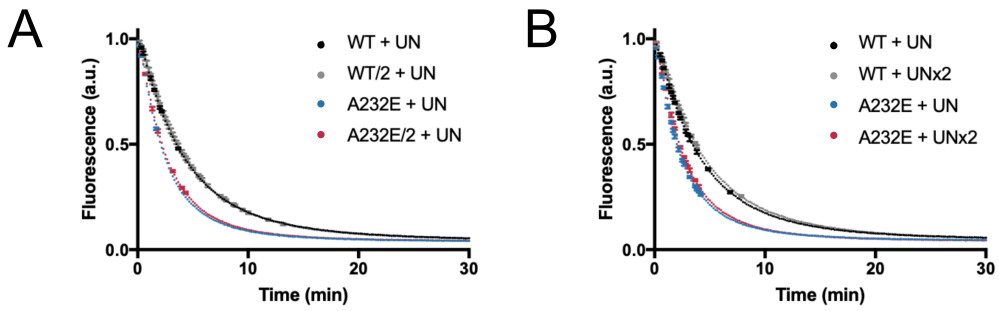

Figure 4.3: Single-turnover assays are at saturating concentrations of p97 and UN. (A) When the concentration of p97 is halved, the rate of unfolding of WT is 98.5% ± 0.4% of original, while the rate of unfolding of A232E is 93.7% ± 0.4% of original. (B) When the concentration of UN is doubled, the rate of unfolding of WT is 92.7% ± 0.3% of original, while the rate of unfolding of A232E is 93% ± 1% of original. Rates were determined from single exponential fits. Error bars represent S.D. with n=3.

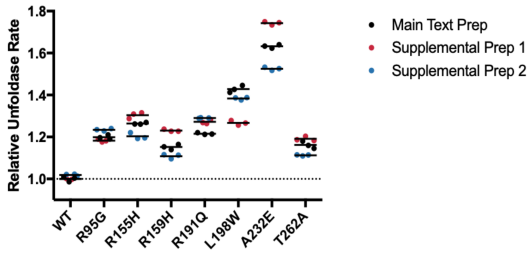

Figure 4.4: Prep-to-prep variability in MSP mutant unfoldase rates. All MSP mutations showed increased unfoldase rates compared to WT, but large prep-to-prep variability exists within mutant proteins. For supplementary preps, all rates were normalized to that of WT Supplementary Prep 1, and assays were carried out in a modified assay buffer under slightly different conditions than the main text prep (see Methods). The main text prep rates are repeated from Figure 4.2B.

Given the variability among protein preparations from our heterologous expression system, we wanted to investigate whether the observed enhancement in MSP mutants can be recapitulated in proteins made in mammalian cells. To do so, we expressed and purified p97-FLAG from Expi293 cells. Compared to a similar

construct from *E. coli*, mammalian-made p97 was significantly faster at unfolding our substrate and was able to unfold without the addition of purified UN (Figure 4.5A). Given that human p97 is decorated with PTMs (*48*, *166*) and p97 from mammalian cells can co-purify with adaptor proteins, these results are not surprising. Importantly, A232E made from a mammalian source is a faster unfoldase than WT made from a mammalian source (Figure 4.5B), suggesting that our observations with bacterially-made proteins is not an artifact. Due to variability among mammalian-expressed protein preparations that are technically difficult to control, such as PTMs and co-purifying proteins, we chose to continue our characterization of MSP mutations using proteins made in *E. coli*.

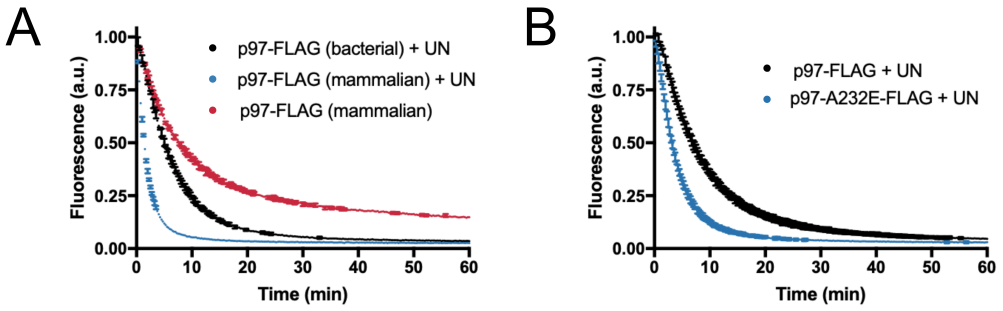

Figure 4.5: Mammalian-made A232E is a faster unfoldase than WT. (A) Mammalian protein is a faster unfoldase than bacterial protein and can promote unfolding without the addition of exogenous UN (red trace). Experiment was carried out at 37 °C with 20 nM substrate, 250 nM p97 hexamer, and 500 nM UN. Error bars represent S.D. with n = 2. (B) Mammalian-made A232E unfolds substrate faster than mammalian-made WT. Experiment was carried out at 25 °C with 20 nM substrate, 2 μM p97 hexamer, and 2 μM UN. Error bars represent S.D. with n=2.

MSP patients are heterozygous, so p97 hexamers comprising a mix of WT and mutant protomers exist in cells. Therefore, we were interested in the ability of mixed hexamers to unfold our model substrate. Three heterogeneous pools of mixed hexamers with increasing ratios of A232E:WT protomers were purified as previously described (Figure 2.7A). Mixed hexamers displayed unfoldase rates between those of pure WT and A232E hexamers, and the unfoldase rate increased as the relative number of mutant protomers increased (Figure 4.6).

ATPase activity does not correlate with unfoldase activity

Previous studies have shown MSP mutants have accelerated basal ATPase activities (*28*, *117*, *118*); therefore, one potential explanation for accelerated unfolding by MSP mutants is that they have simply higher enzymatic activity. To assess this, we first examined the basal ATPase rates of the MSP mutants. As previously reported in the literature, all MSP mutants have higher basal ATPase rates than

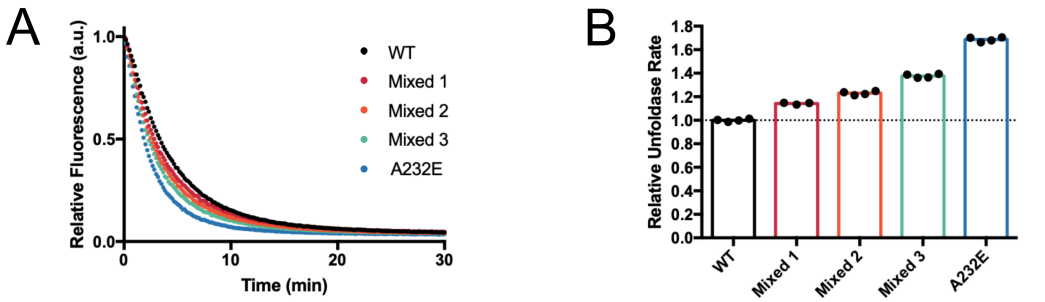

Figure 4.6: Unfoldase rates correlate with the number of mutant subunits in a mixed hexamer. (A) Example single-turnover unfoldase data with mixed hexamer fractions. An SDS-PAGE gel of Mixed 1-3 can be found in Figure 2.7A. (B) Unfoldase data comparing mixed hexamers with pure WT and A232E hexamers. Fluorescence data was fit to a single exponential, and rates were normalized to that of WT. Technical replicates shown with a bar representing the average.

WT (Figure 4.7A). However, while processing substrate, the ATPase activity of p97 is stimulated (*141*, *163*), so a comparison of these rates is more appropriate for assessing a correlation between unfoldase rates and ATPase rates. Under saturating concentrations of UN-substrate, mutants still have a higher ATPase rate than WT, but the effect is much more subtle (up to 1.5-fold compared to 5- to 10-fold) (Figure 4.7B). These stimulated ATPase rates are not well correlated to unfoldase rate (Figure 4.7E), suggesting that mutants are not unfolding substrate faster because they are consuming ATP faster.

Further underscoring this conclusion are similar analyses using mixed WT-A232E hexamers. As expected, the basal ATPase rates of mixed hexamers increase as the average number of mutant protomers in a hexamer increases (Figure 4.7B). However, during substrate processing, all mixed hexamer populations have an essentially identical ATPase rate in comparison to that of WT (Figure 4.7D). The accelerated unfoldase rates of mixed WT-A232E hexamers do not correlate at all to stimulated ATPase rates (Figure 4.7), implying again that ATP hydrolysis is not the cause of accelerated unfolding by MSP mutants.

4.3 Discussion

Here we demonstrate that accelerated unfoldase activity is a defining feature among p97 MSP mutations, supporting a gain of function model for p97-UN processes. Our ATPase analysis of p97 during substrate processing provides strong evidence that the accelerated basal ATPase rates of MSP mutants widely reported in the literature is not a cause of disease but rather is an epiphenomenon. One caveat to our stimulated ATPase assay is that our measurements were taken at time points during which we expect, based on our single turnover rates, that p97 has completed

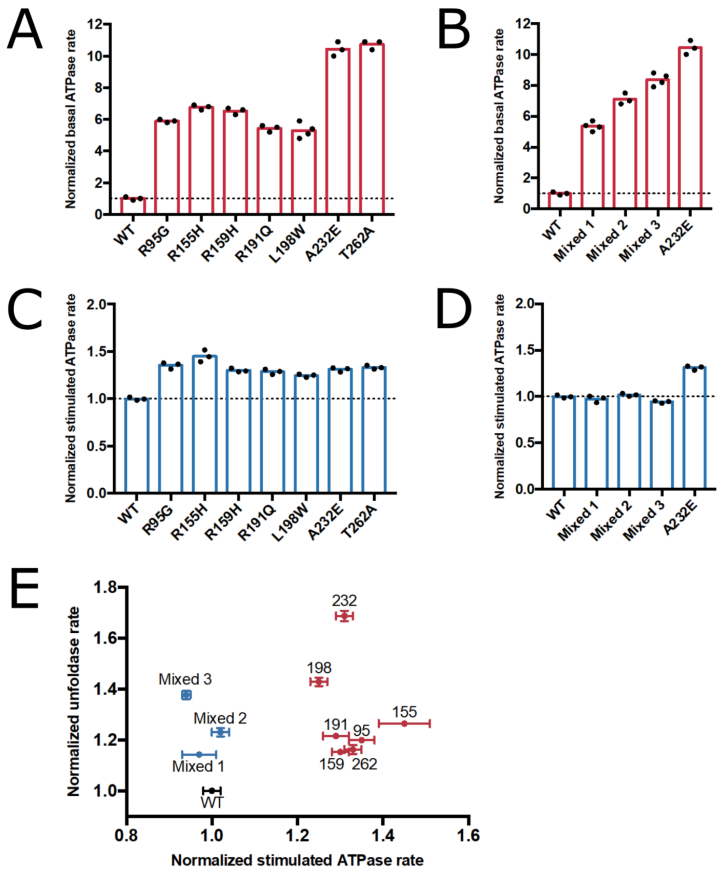

Figure 4.7: MSP mutant ATPase rates do not correlate with unfoldase rates. (A, C) Basal ATPase rates normalized to WT. (B, D) ATPase rates of 50 nM p97 stimulated by the presence of 250 nM UN-substrate, normalized to that of WT (E) Plot of unfoldase rate versus stimulated ATPase rate. All values shown are normalized to WT measurements. N $\geq$ 3 and error bars = s.d. WT and A232E data are repeated among panels.

one round of substrate unfolding. Because we do not include DUBs in our assays (*163*), p97 is likely unable to efficiently turn over substrate, and consequently our measurements may capture ATPase activity while p97 is stalled on ubiquitin chains or otherwise dealing with product inhibition of new substrate unfolding. However, we feel this rate still adequately reflects the ATPase rate while actively engaged by a substrate. With stimulated ATPase rates being similar between WT and mutant hexamers and identical between WT and WT-A232E mixed hexamers, we conclude that ATP hydrolysis is not the rate-determining step of substrate unfolding in our single turnover assays.

If MSP mutants are not hydrolyzing ATP faster, how then do they achieve faster unfoldase rates? In Chapter 2, we discovered a 30- to 60-fold increased UN affinity in mutant and a 10- to 30-fold increased UN affinity in WT-A232E mixed hexamers compared to WT (Table 2.1, 2.2). Structural data suggests that this difference is

caused by a shift in the up/down N domain equilibrium, with mutants favoring the up conformation. Faster binding of UN, and hence faster binding of substrate, could explain the accelerated single turnover rates we observe if the initiation of unfolding is the rate-determining step. All three MSP mutants tested had similar UN affinities in ATP (Table 2.2), yet they displayed unfoldase rates ranging from approximately 120-170% that of WT (Figure 4.2C). NMR studies of the up/down equilibrium of p97 N domains revealed a continuum of perturbations among MSP mutations (*122*), suggesting subtle differences in structure that could further affect substrate engagement beyond UN binding. With such high UN affinity, mutants likely have a disparate rate-determining step than WT that gives rise to rate differences. More detailed mechanistic studies are needed to fully explore the kinetics of substrate unfolding by p97 and how they are perturbed by MSP mutations.

MSP mutations are dominant, and this inheritance pattern could be explained by a gain of function model or by a dominant negative model whereby mutant protomers poison WT hexamers. We demonstrated that mixed WT-mutant hexamers are fully functional and, like pure mutant hexamers, display faster unfolding than WT, lending evidence to support a gain of function model for UN-dependent processes. These biochemical results support a few potential models for MSP pathology. First, an increase in UN binding from perturbed up/down N-domain equilibrium could cause disease by enhancing p97-UN-dependent processes, leading to the inappropriate degradation of protein targets. Some support for this model exists in the MSP literature. Studies on a mouse model of MSP demonstrated increased turnover of IκB-α, leading to the improper activation of NF-κB signaling (*110*). Degradation of IκB-α is dependent upon the p97-UN complex, suggesting that overactivation of p97-UN could explain this phenotype (*84*, *167*, *168*). Similarly, increased processing of TDP-43 and mitofusion in MSP mutants have been demonstrated in *Drosophila* (*108*, *169*). Another consequence of p97-UN overactivation could be the formation of detrimental aggregates if the proteasome is unable to handle an increase in unfolded protein products. Aggregates decorated with ubiquitin are found in tissues affected by MSP (*84*), suggesting an overburdened proteasome.

However, the p97 system is extremely complex, and we cannot discount other hypothesis for MSP pathology that are consistent with our biochemistry. An alternative hypothesis for disease is that the adaptor imbalance itself causes problems for the cell. Based on published estimations (*87*, *170*, *171*) and our affinity measurements, in WT cells we expect intracellular concentrations to be

approximately 60 nM free UN, 420 nM free p97, and 80 nM p97-UN complex. However, in the mutant cells we would expect essentially all of the UN to be in complex with p97, forming intracellular concentrations of 360 nM free p97 and 140 nM p97-UN complex. If free UN is necessary for initial substrate binding, as has been suggested for mitophagy (*97*), the lack of this pool in mutant cells could cause a loss of p97-UN dependent functions. Alternatively, with less free p97 available to bind other adaptors, this imbalance of UN binding could cause a loss of function in other p97-dependent pathways (*116*, *125*). Additionally, we cannot rule out that our gain of p97-UN function is an epiphenomenon whereas gain or loss of function with another p97 adaptor is responible for pathology. In particular, UBXD1 has decreased binding to MSP mutants due to their preference for the N domain down conformation (*58*, *121*, *122*), and failures in lysosomal degradation have been associated with MSP mutations (*58*, *103*, *107*, *172*).

If indeed MSP is caused by a gain of function in p97-UN-dependent pathways, a p97 inhibitor could be an effective treatment for MSP. Though an inhibitor would not rectify the causal defect—abberant N domain conformations and adaptor binding—it would minimize the harmful downstream effects of increased UN binding. We demonstrated this proof of concept by showing that a low concentration of the p97 inhibitor CB-5083 was able to restore WT-like unfolding in the MSP mutant A232E in vitro (*141*). Such an approach was also demonstrated to be viable in *Drosophila*, where physiological and morphological defects in muscle tissue caused by the expression of mutant p97 were reversed through treatment with low doses of p97 inhibitor (*108*). Currently, there is no treatment for MSP, but our biochemical work suggests an exciting potential therapeutic avenue. More cell-based experiments are needed to distinguish among these hypotheses to identify the molecular basis for MSP pathology and explore whether p97 inhibitors may be effective treatments.

4.4 Methods

Protein expression and purification

Expression, purification, and labeling of UN and p97-His were carried out as previously described (*141*). MSP mutations of these constructs were carried out using site-directed mutagenesis and prepared like WT.

A plasmid encoding p97-A232E-FLAG was made through site directed mutagenesis of a plasmid encoding WT p97-FLAG under the CMV promoter (RDB#2946).

Expi293 suspension cells were grown in Expi293 Expression Medium (Thermo Fisher) at 37°C with 8% CO_2. Cells were transfected with 1.1 mg DNA per 1 L of cells using polyethyleneimine "Max" (MW 40,000) (Polysciences) at a ratio of 1:2.7 DNA:PEI. After 72 hours, cells were harvested at 3000g for 15 minutes and washed once with 30 mL cold PBS. Cell pellet was resuspended in lysis buffer (50 mM Tris pH 7.4, 150 mM KCl, 5 mM $MgCl_2$, 5% glycerol, 0.5% Triton X-100) with protease inhibitors (Roche) and incubated with rotation at 4 °C for 30 minutes. Clarified lysate was incubated with 2 mL of anti-FLAG resin (Sigma) at 4 °C for 1.5 hours. Resin was washed with three column volumes of wash buffer (50 mM Tris pH 7.4, 400 mM KCl, 5 mM $MgCl_2$, 0.5% Triton X-100) three times for ten minutes with rotation followed by one wash with elution buffer without FLAG peptide (25 mM Hepes pH 7.4, 150 mM KCl, 2 mM $MgCl_2$). Protein was eluted with 2 mL of elution buffer containing 0.2 mg/mL 3XFLAG peptide for ten minutes with rotation. Elution was repeated, and resin was drained with a final 2 mL of elution buffer. Protein was concentrated and exchanged into storage buffer (20 mM Hepes pH 7.4, 250 mM KCl, 1 mM $MgCl_2$, 5% glycerol, 0.5 mM TCEP) before flash freezing.

Substrate preparation

His_6-Ub^{G76V}-Ub^{G76V}-mEos3.2 was constructed by replacing GFP in the previously published His_6-Ub^{G76V}-Ub^{G76V}-GFP substrate (RDB 3344) (*141*) with a PCR amplicon of mEos3.2 using BamHI and NotI restriction sites. Protein was expressed in BL21(DE3) overnight at 18 °C. Cells were lysed by sonication in 50 mM Tris pH 8.0, 250 mM NaCl, 20 mM imidazole, 2 mM 2-mercaptoethanol, and protease inhibitors (Roche), and clarified lysate was incubated with Ni-NTA resin for 2 hours at 4 °C. After elution from the resin with 200 mM imidazole, protein was spin concentrated and dialyzed overnight into 50 mM Hepes pH 7.0, 150 mM NaCl, 2 mM 2-mercaptoethanol. Sample was irradiated with 380 nm LED light (Thorlabs) for one hour at 4 °C. After filtration, protein was purified on a Superdex 200 column (20 mM Hepes pH 7.4, 100 mM KCl, 3 mM $MgCl_2$), and fractions were pooled, concentrated and flash frozen. Ubiquitylation and purification of the ubiquitylated substrate was carried out as previously described (*141*). Final substrate showed approximately 40% photocleavage as measured by absorbance at 507 and 572 nm (*162*). Concentrations of substrate referred to in this paper correspond to the concentration of photocleaved (red) protein.

Unfoldase assays

Experiments were carried out in Assay Buffer (20 mM Hepes pH 7.4, 150 mM KCl, 20 mM $MgCl_2$, 1 mM TCEP, 1 mg/mL BSA) supplemented with ATP regeneration system (5 mM ATP, 30 mM creatine phosphate, 50 μg/mL creatine phosphokinase). Proteins were preincubated in a 96-well plate (Costar 3694) for 15 minutes at 37 °C before the addition of ATP regeneration system to initiate the reaction. Final concentrations were 20 nM substrate, 400 nM p97 hexamer, and 800 nM UN. Fluorescence was read on a PHERAstar Plus (BMG Labtech) or Synergy Neo2 (BioTek) plate reader using a 540 nm excitation filter and 590 nm emission filter. Data were normalized to the first reading and fit to a single exponential decay equation to extract an unfolding rate.

ATPase assays

Proteins (100-400 nM p97) were diluted in assay buffer and preincubated in a 96-well plate (Costar 3695) for 10 minutes at 37 °C before the addition of ATPase mix (5 mM ATP, 1 mM NADH, 7.5 mM PEP, 50X dilution PK/LDH (Sigma P0294)). For stimulated ATPase rates, final concentrations were 50 nM p97, 250 nM UN, and 250 nM substrate. After 15 minutes, A_{340} was monitored for ten minutes, converted to an NADH concentration, and fit to a line to determine the ATPase rate. A WT p97 control was included in every plate and used to normalize ATPase rates.

BIBLIOGRAPHY

(*1*) Balch, W. E., Morimoto, R. I., Dillin, A., and Kelly, J. W., (Feb. 2008). Adapting Proteostasis for Disease Intervention. *Science 319*, 916–919.

(*2*) Vilchez, D., Saez, I., and Dillin, A., (Dec. 2014). The role of protein clearance mechanisms in organismal ageing and age-related diseases. *Nature Communications 5*.

(*3*) Deshaies, R. J., (Dec. 2014). Proteotoxic crisis, the ubiquitin-proteasome system, and cancer therapy. *BMC Biology 12*.

(*4*) Kleiger, G., and Mayor, T., (June 2014). Perilous journey: a tour of the ubiquitin–proteasome system. *Trends in Cell Biology 24*, 352–359.

(*5*) Chau, V., Tobias, J., Bachmair, A., Marriott, D., Ecker, D., Gonda, D., and Varshavsky, A., (Mar. 1989). A multiubiquitin chain is confined to specific lysine in a targeted short-lived protein. *Science 243*, 1576–1583.

(*6*) Swatek, K. N., and Komander, D., (2016). Ubiquitin modifications. *Cell research 26*, 399–422.

(*7*) Finley, D., Sadis, S., Monia, B. P., Boucher, P., Ecker, D. J., Crooke, S. T., and Chau, V., (Aug. 1994). Inhibition of proteolysis and cell cycle progression in a multiubiquitination-deficient yeast mutant. *Molecular and Cellular Biology 14*, 5501–5509.

(*8*) Thrower, J. S., Hoffman, L., Rechsteiner, M., and Pickart, C. M., (Jan. 2000). Recognition of the polyubiquitin proteolytic signal. *The EMBO journal 19*, 94–102.

(*9*) Inobe, T., and Matouschek, A., (Feb. 2014). Paradigms of protein degradation by the proteasome. *Current Opinion in Structural Biology 24*, 156–164.

(*10*) van den Boom, J., and Meyer, H., (Jan. 2018). VCP/p97-Mediated Unfolding as a Principle in Protein Homeostasis and Signaling. *Molecular Cell 69*, 182–194.

(*11*) Stach, L., and Freemont, P. S., (Sept. 2017). The AAA+ ATPase p97, a cellular multitool. *Biochemical Journal 474*, 2953–2976.

(*12*) Wolf, D. H., and Stolz, A., (Jan. 2012). The Cdc48 machine in endoplasmic reticulum associated protein degradation. *Biochimica et Biophysica Acta (BBA) - Molecular Cell Research 1823*, 117–124.

(*13*) Alverez, C., et al. (Feb. 2016). Allosteric Indole Amide Inhibitors of p97: Identification of a Novel Probe of the Ubiquitin Pathway. *ACS Medicinal Chemistry Letters 7*, 182–187.

(*14*) Magnaghi, P., et al. (Sept. 2013). Covalent and allosteric inhibitors of the ATPase VCP/p97 induce cancer cell death. *Nature Chemical Biology 9*, 548–556.

(*15*) Anderson, D. J., et al. (Nov. 2015). Targeting the AAA ATPase p97 as an Approach to Treat Cancer through Disruption of Protein Homeostasis. *Cancer Cell 28*, 653–665.

(*16*) Ding, R., Zhang, T., Wilson, D. J., Xie, J., Williams, J., Xu, Y., Ye, Y., and Chen, L., (Mar. 2019). Discovery of Irreversible p97 Inhibitors. *Journal of Medicinal Chemistry 62*, 2814–2829.

(*17*) LaPorte, M. G., Burnett, J. C., Colombo, R., Bulfer, S. L., Alverez, C., Chou, T.-F., Neitz, R. J., Green, N., Moore, W. J., Yue, Z., Li, S., Arkin, M. R., Wipf, P., and Huryn, D. M., (Nov. 2018). Optimization of Phenyl Indole Inhibitors of the AAA+ ATPase p97. *ACS Medicinal Chemistry Letters 9*, 1075–1081.

(*18*) Chou, T.-F., Brown, S. J., Minond, D., Nordin, B. E., Li, K., Jones, A. C., Chase, P., Porubsky, P. R., Stoltz, B. M., Schoenen, F. J., Patricelli, M. P., Hodder, P., Rosen, H., and Deshaies, R. J., (Mar. 2011). Reversible inhibitor of p97, DBeQ, impairs both ubiquitin-dependent and autophagic protein clearance pathways. *Proceedings of the National Academy of Sciences 108*, 4834–4839.

(*19*) Chou, T.-F., Li, K., Frankowski, K. J., Schoenen, F. J., and Deshaies, R. J., (Feb. 2013). Structure-Activity Relationship Study Reveals ML240 and ML241 as Potent and Selective Inhibitors of p97 ATPase. *ChemMedChem 8*, 297–312.

(*20*) Vekaria, P. H., Home, T., Weir, S., Schoenen, F. J., and Rao, R., (Aug. 2016). Targeting p97 to Disrupt Protein Homeostasis in Cancer. *Frontiers in Oncology 6*.

(*21*) Meyer, H., Bug, M., and Bremer, S., (Feb. 2012). Emerging functions of the VCP/p97 AAA-ATPase in the ubiquitin system. *Nature Cell Biology 14*, 117–123.

(*22*) Banerjee, S., et al. (Feb. 2016). 2.3 A resolution cryo-EM structure of human p97 and mechanism of allosteric inhibition. *Science 351*, 871–875.

(*23*) Zhang, X., Shaw, A., Bates, P. A., Newman, R. H., Gowen, B., Orlova, E., Gorman, M. A., Kondo, H., Dokurno, P., Lally, J., et al. (2000). Structure of the AAA ATPase p97. *Molecular cell 6*, 1473–1484.

(*24*) Huyton, T., Pye, V. E., Briggs, L. C., Flynn, T. C., Beuron, F., Kondo, H., Ma, J., Zhang, X., and Freemont, P. S., (Dec. 2003). The crystal structure of murine p97/VCP at 3.6Å. *Journal of Structural Biology 144*, 337–348.

(*25*) DeLaBarre, B., and Brunger, A. T., (Mar. 2005). Nucleotide Dependent Motion and Mechanism of Action of p97/VCP. *Journal of Molecular Biology 347*, 437–452.

(*26*) Davies, J. M., Brunger, A. T., and Weis, W. I., (May 2008). Improved Structures of Full-Length p97, an AAA ATPase: Implications for Mechanisms of Nucleotide-Dependent Conformational Change. *Structure 16*, 715–726.

(*27*) Chapman, E., Fry, A. N., and Kang, M., (2011). The complexities of p97 function in health and disease. *Mol. BioSyst. 7*, 700–710.

(*28*) Chou, T.-F., Bulfer, S. L., Weihl, C. C., Li, K., Lis, L. G., Walters, M. A., Schoenen, F. J., Lin, H. J., Deshaies, R. J., and Arkin, M. R., (July 2014). Specific Inhibition of p97/VCP ATPase and Kinetic Analysis Demonstrate Interaction between D1 and D2 ATPase Domains. *Journal of Molecular Biology 426*, 2886–2899.

(*29*) Wang, Q., Song, C., and Li, C.-C. H., (Jan. 2003). Hexamerization of p97-VCP is promoted by ATP binding to the D1 domain and required for ATPase and biological activities. *Biochemical and Biophysical Research Communications 300*, 253–260.

(*30*) Briggs, L. C., Baldwin, G. S., Miyata, N., Kondo, H., Zhang, X., and Freemont, P. S., (May 2008). Analysis of Nucleotide Binding to P97 Reveals the Properties of a Tandem AAA Hexameric ATPase. *Journal of Biological Chemistry 283*, 13745–13752.

(*31*) Yeung, H. O., Forster, A., Bebeacua, C., Niwa, H., Ewens, C., McKeown, C., Zhang, X., and Freemont, P. S., (Mar. 2014). Inter-ring rotations of AAA ATPase p97 revealed by electron cryomicroscopy. *Open Biology 4*, 130142–130142.

(*32*) Song, C., (Jan. 2003). ATPase Activity of p97-Valosin-containing Protein (VCP): D2 mediates the major enzyme activity, and D1 contributes to the heat-induced activity. *Journal of Biological Chemistry 278*, 3648–3655.

(*33*) Ye, Y., (July 2003). Function of the p97-Ufd1-Npl4 complex in retrotranslocation from the ER to the cytosol: dual recognition of nonubiquitinated polypeptide segments and polyubiquitin chains. *The Journal of Cell Biology 162*, 71–84.

(*34*) Beskow, A., Grimberg, K. B., Bott, L. C., Salomons, F. A., Dantuma, N. P., and Young, P., (Dec. 2009). A Conserved Unfoldase Activity for the p97 AAA-ATPase in Proteasomal Degradation. *Journal of Molecular Biology 394*, 732–746.

(*35*) Esaki, M., and Ogura, T., (Feb. 2010). ATP-bound form of the D1 AAA domain inhibits an essential function of Cdc48p/p97This paper is one of a selection of papers published in this special issue entitled 8th International Conference on AAA Proteins and has undergone the Journal's usual peer review process. *Biochemistry and Cell Biology 88*, 109–117.

(*36*) Rouiller, I., Butel, V. M., Latterich, M., Milligan, R. A., and Wilson-Kubalek, E. M., (2000). A major conformational change in p97 AAA ATPase upon ATP binding. *Molecular cell 6*, 1485–1490.

(*37*) Rouiller, I., DeLaBarre, B., May, A. P., Weis, W. I., Brunger, A. T., Milligan, R. A., and Wilson-Kubalek, E. M., (Dec. 2002). Conformational changes of the multifunction p97 AAA ATPase during its ATPase cycle. *Nature Structural Biology 9*, 950–957.

(*38*) Beuron, F., Flynn, T. C., Ma, J., Kondo, H., Zhang, X., and Freemont, P. S., (Mar. 2003). Motions and Negative Cooperativity Between p97 Domains Revealed by Cryo-electron Microscopy and Quantised Elastic Deformational Model. *Journal of Molecular Biology 327*, 619–629.

(*39*) Davies, J. M., Tsuruta, H., May, A. P., and Weis, W. I., (Feb. 2005). Conformational Changes of p97 during Nucleotide Hydrolysis Determined by Small-Angle X-Ray Scattering. *Structure 13*, 183–195.

(*40*) Noi, K., Yamamoto, D., Nishikori, S., Arita-Morioka, K.-i., Kato, T., Ando, T., and Ogura, T., (Nov. 2013). High-Speed Atomic Force Microscopic Observation of ATP-Dependent Rotation of the AAA+ Chaperone p97. *Structure 21*, 1992–2002.

(*41*) Tang, W. K., and Xia, D., (Jan. 2016). Role of the D1-D2 Linker of Human VCP/p97 in the Asymmetry and ATPase Activity of the D1-domain. *Scientific Reports 6*, 20037.

(*42*) Schuller, J. M., Beck, F., Lössl, P., Heck, A. J. R., and Förster, F., (Mar. 2016). Nucleotide-dependent conformational changes of the AAA+ ATPase p97 revisited. *FEBS Letters 590*, 595–604.

(*43*) Hänzelmann, P., and Schindelin, H., (Jan. 2016). Structural Basis of ATP Hydrolysis and Intersubunit Signaling in the AAA+ ATPase p97. *Structure 24*, 127–139.

(*44*) Nishikori, S., Esaki, M., Yamanaka, K., Sugimoto, S., and Ogura, T., (May 2011). Positive Cooperativity of the p97 AAA ATPase Is Critical for Essential Functions. *Journal of Biological Chemistry 286*, 15815–15820.

(*45*) Huang, C., Li, G., and Lennarz, W. J., (June 2012). Dynamic flexibility of the ATPase p97 is important for its interprotomer motion transmission. *Proceedings of the National Academy of Sciences 109*, 9792–9797.

(*46*) Li, G., Huang, C., Zhao, G., and Lennarz, W. J., (2012). Interprotomer motion-transmission mechanism for the hexameric AAA ATPase p97. *Proceedings of the National Academy of Sciences 109*, 3737–3741.

(*47*) Zhang, X., et al. (Apr. 2015). Altered cofactor regulation with disease-associated p97/VCP mutations. *Proceedings of the National Academy of Sciences 112*, E1705–E1714.

(*48*) Hänzelmann, P., and Schindelin, H., (Apr. 2017). The Interplay of Cofactor Interactions and Post-translational Modifications in the Regulation of the AAA+ ATPase p97. *Frontiers in Molecular Biosciences 4*.

(*49*) Alexandru, G., Graumann, J., Smith, G. T., Kolawa, N. J., Fang, R., and Deshaies, R. J., (Sept. 2008). UBXD7 Binds Multiple Ubiquitin Ligases and Implicates p97 in HIF1alpha Turnover. *Cell 134*, 804–816.

(*50*) Hänzelmann, P., Buchberger, A., and Schindelin, H., (June 2011). Hierarchical Binding of Cofactors to the AAA ATPase p97. *Structure 19*, 833–843.

(*51*) Schuberth, C., and Buchberger, A., (Aug. 2008). UBX domain proteins: major regulators of the AAA ATPase Cdc48/p97. *Cellular and Molecular Life Sciences 65*, 2360–2371.

(*52*) Meyer, H. H., Wang, Y., and Warren, G., (2002). Direct binding of ubiquitin conjugates by the mammalian p97 adaptor complexes, p47 and Ufd1–Npl4. *The EMBO journal 21*, 5645–5652.

(*53*) Wang, Y., (Mar. 2004). VCIP135 acts as a deubiquitinating enzyme during p97-p47-mediated reassembly of mitotic Golgi fragments. *The Journal of Cell Biology 164*, 973–978.

(*54*) Liu, Y., and Ye, Y., (2012). Roles of p97-associated deubiquitinases in protein quality control at the endoplasmic reticulum. *Current protein & peptide science 13*, 436.

(*55*) Wang, Q., Li, L., and Ye, Y., (Sept. 2006). Regulation of retrotranslocation by p97-associated deubiquitinating enzyme ataxin-3. *The Journal of Cell Biology 174*, 963–971.

(*56*) Ernst, R., Mueller, B., Ploegh, H. L., and Schlieker, C., (Oct. 2009). The Otubain YOD1 Is a Deubiquitinating Enzyme that Associates with p97 to Facilitate Protein Dislocation from the ER. *Molecular Cell 36*, 28–38.

(*57*) Totsukawa, G., Kaneko, Y., Uchiyama, K., Toh, H., Tamura, K., and Kondo, H., (Aug. 2011). VCIP135 deubiquitinase and its binding protein, WAC, in p97ATPase-mediated membrane fusion. *The EMBO journal 30*, 3581–3593.

(*58*) Ritz, D., Vuk, M., Kirchner, P., Bug, M., Schütz, S., Hayer, A., Bremer, S., Lusk, C., Baloh, R. H., Lee, H., Glatter, T., Gstaiger, M., Aebersold, R., Weihl, C. C., and Meyer, H., (Aug. 2011). Endolysosomal sorting of ubiquitylated caveolin-1 is regulated by VCP and UBXD1 and impaired by VCP disease mutations. *Nature Cell Biology 13*, 1116–1123.

(*59*) Verma, R., Oania, R., Fang, R., Smith, G. T., and Deshaies, R. J., (Jan. 2011). Cdc48/p97 mediates UV-dependent turnover of RNA Pol II. *Molecular Cell 41*, 82–92.

(*60*) Besten, W. d., Verma, R., Kleiger, G., Oania, R. S., and Deshaies, R. J., (Apr. 2012). NEDD8 links cullin-RING ubiquitin ligase function to the p97 pathway. *Nature Structural & Molecular Biology 19*, 511–516.

(*61*) Raman, M., Sergeev, M., Garnaas, M., Lydeard, J. R., Huttlin, E. L., Goessling, W., Shah, J. V., and Harper, J. W., (Sept. 2015). Systematic proteomics of the VCP–UBXD adaptor network identifies a role for UBXN10 in regulating ciliogenesis. *Nature Cell Biology 17*, 1356–1369.

(*62*) Rezvani, K., Teng, Y., Pan, Y., Dani, J. A., Lindstrom, J., Garcia Gras, E. A., McIntosh, J. M., and De Biasi, M., (May 2009). UBXD4, a UBX-Containing Protein, Regulates the Cell Surface Number and Stability of 3-Containing Nicotinic Acetylcholine Receptors. *Journal of Neuroscience 29*, 6883–6896.

(*63*) Kondo, H., Rabouille, C., Newman, R., Levine, T. P., Pappin, D., Freemont, P., and Warren, G., (1997). p47 is a cofactor for p97-mediated membrane fusion. *Nature 388*, 75–78.

(*64*) Huang, S., Tang, D., and Wang, Y., (July 2016). Monoubiquitination of Syntaxin 5 Regulates Golgi Membrane Dynamics during the Cell Cycle. *Developmental Cell 38*, 73–85.

(*65*) Meyer, H. H., Shorter, J. G., Seemann, J., Pappin, D., and Warren, G., (2000). A complex of mammalian Ufd1 and Npl4 links the AAA-ATPase, p97, to ubiquitin and nuclear transport pathways. *The EMBO journal 19*, 2181–2192.

(*66*) Ewens, C. A., Panico, S., Kloppsteck, P., McKeown, C., Ebong, I.-O., Robinson, C., Zhang, X., and Freemont, P. S., (Apr. 2014). The p97-FAF1 Protein Complex Reveals a Common Mode of p97 Adaptor Binding. *Journal of Biological Chemistry 289*, 12077–12084.

(*67*) Bodnar, N. O., Kim, K. H., Ji, Z., Wales, T. E., Svetlov, V., Nudler, E., Engen, J. R., Walz, T., and Rapoport, T. A., (July 2018). Structure of the Cdc48 ATPase with its ubiquitin-binding cofactor Ufd1–Npl4. *Nature Structural & Molecular Biology*.

(*68*) Arumughan, A., et al. (Oct. 2016). Quantitative interaction mapping reveals an extended UBX domain in ASPL that disrupts functional p97 hexamers. *Nature Communications 7*, 13047.

(*69*) Rijal, R., Arhzaouy, K., Strucksberg, K.-H., Cross, M., Hofmann, A., Schröder, R., Clemen, C. S., and Eichinger, L., (June 2016). Mutant p97 exhibits species-specific changes of its ATPase activity and compromises the UBXD9-mediated monomerisation of p97 hexamers. *European Journal of Cell Biology 95*, 195–207.

(*70*) Trusch, F., Matena, A., Vuk, M., Koerver, L., Knævelsrud, H., Freemont, P. S., Meyer, H., and Bayer, P., (Dec. 2015). The N-terminal Region of the Ubiquitin Regulatory X (UBX) Domain-containing Protein 1 (UBXD1) Modulates Interdomain Communication within the Valosin-containing Protein p97. *Journal of Biological Chemistry 290*, 29414–29427.

(*71*) Hanzelmann, P., and Schindelin, H., (Nov. 2011). The Structural and Functional Basis of the p97/Valosin-containing Protein (VCP)-interacting Motif (VIM): mutually exclusive binding of cofactors to the N-terminal domain of p97. *Journal of Biological Chemistry 286*, 38679–38690.

(*72*) Dreveny, I., Kondo, H., Uchiyama, K., Shaw, A., Zhang, X., and Freemont, P. S., (2004). Structural basis of the interaction between the AAA ATPase p97/VCP and its adaptor protein p47. *The EMBO journal 23*, 1030–1039.

(*73*) Kim, K. H., Kang, W., Suh, S. W., and Yang, J. K., (Aug. 2011). Crystal structure of FAF1 UBX domain in complex with p97/VCP N domain reveals a conformational change in the conserved FcisP touch-turn motif of UBX domain. *Proteins: Structure, Function, and Bioinformatics 79*, 2583–2587.

(*74*) Stapf, C., Cartwright, E., Bycroft, M., Hofmann, K., and Buchberger, A., (Nov. 2011). The General Definition of the p97/Valosin-containing Protein (VCP)-interacting Motif (VIM) Delineates a New Family of p97 Cofactors. *Journal of Biological Chemistry 286*, 38670–38678.

(*75*) Le, L. T. M., Kang, W., Kim, J.-Y., Le, O. T. T., Lee, S. Y., and Yang, J. K., (Sept. 2016). Structural Details of Ufd1 Binding to p97 and Their Functional Implications in ER-Associated Degradation. *PLOS ONE 11*, ed. by Brodsky, J. L., e0163394.

(*76*) Beuron, F., Dreveny, I., Yuan, X., Pye, V. E., McKeown, C., Briggs, L. C., Cliff, M. J., Kaneko, Y., Wallis, R., Isaacson, R. L., Ladbury, J. E., Matthews, S. J., Kondo, H., Zhang, X., and Freemont, P. S., (May 2006). Conformational changes in the AAA ATPase p97-p47 adaptor complex. *The EMBO journal 25*, 1967–1976.

(*77*) Pye, V. E., Beuron, F., Keetch, C. A., McKeown, C., Robinson, C. V., Meyer, H. H., Zhang, X., and Freemont, P. S., (2007). Structural insights into the p97-Ufd1-Npl4 complex. *Proceedings of the National Academy of Sciences 104*, 467–472.

(*78*) Bebeacua, C., Förster, A., McKeown, C., Meyer, H. H., Zhang, X., and Freemont, P. S., (2012). Distinct conformations of the protein complex p97-Ufd1-Npl4 revealed by electron cryomicroscopy. *Proceedings of the National Academy of Sciences 109*, 1098–1103.

(*79*) Meyer, H. H., Kondo, H., and Warren, G., (Oct. 1998). The p47 co-factor regulates the ATPase activity of the membrane fusion protein, p97. *FEBS letters 437*, 255–257.

(*80*) Bruderer, R. M., Brasseur, C., and Meyer, H. H., (Nov. 2004). The AAA ATPase p97/VCP Interacts with Its Alternative Co-factors, Ufd1-Npl4 and p47, through a Common Bipartite Binding Mechanism. *Journal of Biological Chemistry 279*, 49609–49616.

(*81*) Watts, G. D. J., Wymer, J., Kovach, M. J., Mehta, S. G., Mumm, S., Darvish, D., Pestronk, A., Whyte, M. P., and Kimonis, V. E., (Apr. 2004). Inclusion body myopathy associated with Paget disease of bone and frontotemporal dementia is caused by mutant valosin-containing protein. *Nature Genetics 36*, 377–381.

(*82*) Johnson, J. O., et al. (Dec. 2010). Exome Sequencing Reveals VCP Mutations as a Cause of Familial ALS. *Neuron 68*, 857–864.

(*83*) Tang, W. K., and Xia, D., (Dec. 2016). Mutations in the Human AAA+ Chaperone p97 and Related Diseases. *Frontiers in Molecular Biosciences 3*, DOI: 10.3389/fmolb.2016.00079.

(*84*) Nalbandian, A., Donkervoort, S., Dec, E., Badadani, M., Katheria, V., Rana, P., Nguyen, C., Mukherjee, J., Caiozzo, V., Martin, B., Watts, G. D., Vesa, J., Smith, C., and Kimonis, V. E., (Nov. 2011). The Multiple Faces of Valosin-Containing Protein-Associated Diseases: Inclusion Body Myopathy with Paget's Disease of Bone, Frontotemporal Dementia, and Amyotrophic Lateral Sclerosis. *Journal of Molecular Neuroscience 45*, 522–531.

(*85*) Al-Obeidi, E., Al-Tahan, S., Surampalli, A., Goyal, N., Wang, A., Hermann, A., Omizo, M., Smith, C., Mozaffar, T., and Kimonis, V., (Jan. 2018). Genotype-phenotype study in patients with valosin-containing protein mutations associated with multisystem proteinopathy. *Clinical Genetics 93*, 119–125.

(*86*) Saracino, D., et al. (June 2018). Novel VCP mutations expand the mutational spectrum of frontotemporal dementia. *Neurobiology of Aging*.

(*87*) Xue, L., Blythe, E. E., Freiberger, E. C., Mamrosh, J. L., Hebert, A. S., Reitsma, J. M., Hess, S., Coon, J. J., and Deshaies, R. J., (Sept. 2016). Valosin-containing protein (VCP)–Adaptor Interactions are Exceptionally Dynamic and Subject to Differential Modulation by a VCP Inhibitor. *Molecular & Cellular Proteomics 15*, 2970–2986.

(*88*) Weber-Ban, E. U., Reid, B. G., Miranker, A. D., and Horwich, A. L., (1999). Global unfolding of a substrate protein by the Hsp100 chaperone ClpA. *Nature 401*, 90–93.

(*89*) Förster, F., Schuller, J., Unverdorben, P., and Aufderheide, A., (Aug. 2014). Emerging Mechanistic Insights into AAA Complexes Regulating Proteasomal Degradation. *Biomolecules 4*, 774–794.

(*90*) Liu, C.-w., Millen, L., Roman, T. B., Xiong, H., Gilbert, H. F., Noiva, R., DeMartino, G. N., and Thomas, P. J., (July 2002). Conformational Remodeling of Proteasomal Substrates by PA700, the 19 S Regulatory Complex of the 26 S Proteasome. *Journal of Biological Chemistry 277*, 26815–26820.

(*91*) Gerega, A., Rockel, B., Peters, J., Tamura, T., Baumeister, W., and Zwickl, P., (Dec. 2005). VAT, the Thermoplasma Homolog of Mammalian p97/VCP, Is an N Domain-regulated Protein Unfoldase. *Journal of Biological Chemistry 280*, 42856–42862.

(*92*) Barthelme, D., and Sauer, R. T., (2012). Identification of the Cdc48• 20S proteasome as an ancient AAA+ proteolytic machine. *Science 337*, 843–846.

(*93*) Zhao, M., Wu, S., Zhou, Q., Vivona, S., Cipriano, D. J., Cheng, Y., and Brunger, A. T., (Jan. 2015). Mechanistic insights into the recycling machine of the SNARE complex. *Nature 518*, 61–67.

(*94*) Hinnerwisch, J., Fenton, W. A., Furtak, K. J., Farr, G. W., and Horwich, A. L., (July 2005). Loops in the Central Channel of ClpA Chaperone Mediate Protein Binding, Unfolding, and Translocation. *Cell 121*, 1029–1041.

(*95*) DeLaBarre, B., Christianson, J. C., Kopito, R. R., and Brunger, A. T., (May 2006). Central Pore Residues Mediate the p97/VCP Activity Required for ERAD. *Molecular Cell 22*, 451–462.

(*96*) Bays, N. W., Wilhovsky, S. K., Goradia, A., Hodgkiss-Harlow, K., and Hampton, R. Y., (Dec. 2001). HRD4/NPL4 is required for the proteasomal processing of ubiquitinated ER proteins. *Molecular Biology of the Cell 12*, 4114–4128.

(*97*) Kimura, Y., Fukushi, J., Hori, S., Matsuda, N., Okatsu, K., Kakiyama, Y., Kawawaki, J., Kakizuka, A., and Tanaka, K., (Dec. 2013). Different dynamic movements of wild-type and pathogenic VCPs and their cofactors to damaged mitochondria in a Parkin-mediated mitochondrial quality control system. *Genes to Cells 18*, 1131–1143.

(*98*) Johnson, E. S., Ma, P. C., Ota, I. M., and Varshavsky, A., (July 1995). A proteolytic pathway that recognizes ubiquitin as a degradation signal. *The Journal of Biological Chemistry 270*, 17442–17456.

(*99*) Prakash, S., Tian, L., Ratliff, K. S., Lehotzky, R. E., and Matouschek, A., (Sept. 2004). An unstructured initiation site is required for efficient proteasome-mediated degradation. *Nature Structural & Molecular Biology 11*, 830–837.

(*100*) Heidelberger, J. B., Voigt, A., Borisova, M. E., Petrosino, G., Ruf, S., Wagner, S. A., and Beli, P., (Apr. 2018). Proteomic profiling of VCP substrates links VCP to K6-linked ubiquitylation and c-Myc function. *EMBO reports 19*, e44754.

(*101*) Liu, C., Liu, W., Ye, Y., and Li, W., (Feb. 2017). Ufd2p synthesizes branched ubiquitin chains to promote the degradation of substrates modified with atypical chains. *Nature Communications 8*, 14274.

(*102*) Meyer, H.-J., and Rape, M., (May 2014). Enhanced Protein Degradation by Branched Ubiquitin Chains. *Cell 157*, 910–921.

(*103*) Ju, J.-S., Fuentealba, R. A., Miller, S. E., Jackson, E., Piwnica-Worms, D., Baloh, R. H., and Weihl, C. C., (Dec. 2009). Valosin-containing protein (VCP) is required for autophagy and is disrupted in VCP disease. *The Journal of Cell Biology 187*, 875–888.

(*104*) Tresse, E., Salomons, F. A., Vesa, J., Bott, L. C., Kimonis, V., Yao, T.-P., Dantuma, N. P., and Taylor, J. P., (Feb. 2010). VCP/p97 is essential for maturation of ubiquitin-containing autophagosomes and this function is impaired by mutations that cause IBMPFD. *Autophagy 6*, 217–227.

(*105*) Ramanathan, H. N., and Ye, Y., (2012). The p97 ATPase associates with EEA1 to regulate the size of early endosomes. *Cell research 22*, 346–359.

(*106*) Ching, J. K., Elizabeth, S. V., Ju, J.-S., Lusk, C., Pittman, S. K., and Weihl, C. C., (Mar. 2013). mTOR dysfunction contributes to vacuolar pathology and weakness in valosin-containing protein associated inclusion body myopathy. *Human Molecular Genetics 22*, 1167–1179.

(*107*) Papadopoulos, C., Kirchner, P., Bug, M., Grum, D., Koerver, L., Schulze, N., Poehler, R., Dressler, A., Fengler, S., Arhzaouy, K., Lux, V., Ehrmann, M., Weihl, C. C., and Meyer, H., (Jan. 2017). VCP/p97 cooperates with YOD1, UBXD1 and PLAA to drive clearance of ruptured lysosomes by autophagy. *The EMBO Journal 36*, 135–150.

(*108*) Zhang, T., Mishra, P., Hay, B. A., Chan, D., and Guo, M., (2017). Valosin-containing protein (VCP/p97) inhibitors relieve Mitofusin-dependent mitochondrial defects due to VCP disease mutants. *eLife 6*, e17834.

(*109*) Johnson, A. E., Shu, H., Hauswirth, A. G., Tong, A., and Davis, G. W., (July 2015). VCP-dependent muscle degeneration is linked to defects in a dynamic tubular lysosomal network in vivo. *eLife 4*.

(*110*) Custer, S. K., Neumann, M., Lu, H., Wright, A. C., and Taylor, J. P., (May 2010). Transgenic mice expressing mutant forms VCP/p97 recapitulate the full spectrum of IBMPFD including degeneration in muscle, brain and bone. *Human Molecular Genetics 19*, 1741–1755.

(*111*) Bartolome, F., et al. (Apr. 2013). Pathogenic VCP Mutations Induce Mitochondrial Uncoupling and Reduced ATP Levels. *Neuron 78*, 57–64.

(*112*) Ju, J.-S., Miller, S. E., Hanson, P. I., and Weihl, C. C., (Oct. 2008). Impaired Protein Aggregate Handling and Clearance Underlie the Pathogenesis of p97/VCP-associated Disease. *Journal of Biological Chemistry 283*, 30289–30299.

(*113*) Weihl, C. C., (Dec. 2005). Inclusion body myopathy-associated mutations in p97/VCP impair endoplasmic reticulum-associated degradation. *Human Molecular Genetics 15*, 189–199.

(*114*) Chang, Y.-C., Hung, W.-T., Chang, Y.-C., Chang, H. C., Wu, C.-L., Chiang, A.-S., Jackson, G. R., and Sang, T.-K., (Feb. 2011). Pathogenic VCP/TER94 Alleles Are Dominant Actives and Contribute to Neurodegeneration by Altering Cellular ATP Level in a Drosophila IBMPFD Model. *PLoS Genetics 7*, ed. by Frankel, W. N., e1001288.

(*115*) Zhou, H.-J., et al. (Dec. 2015). Discovery of a First-in-Class, Potent, Selective, and Orally Bioavailable Inhibitor of the p97 AAA ATPase (CB-5083). *Journal of Medicinal Chemistry 58*, 9480–9497.

(*116*) Manno, A., Noguchi, M., Fukushi, J., Motohashi, Y., and Kakizuka, A., (July 2010). Enhanced ATPase activities as a primary defect of mutant valosin-containing proteins that cause inclusion body myopathy associated with Paget disease of bone and frontotemporal dementia. *Genes to Cells*, 911–922.

(*117*) Halawani, D., LeBlanc, A. C., Rouiller, I., Michnick, S. W., Servant, M. J., and Latterich, M., (Aug. 2009). Hereditary Inclusion Body Myopathy-Linked p97/VCP Mutations in the NH2 Domain and the D1 Ring Modulate p97/VCP ATPase Activity and D2 Ring Conformation. *Molecular and Cellular Biology 29*, 4484–4494.

(*118*) Niwa, H., Ewens, C. A., Tsang, C., Yeung, H. O., Zhang, X., and Freemont, P. S., (Mar. 2012). The Role of the N-Domain in the ATPase Activity of the Mammalian AAA ATPase p97/VCP. *Journal of Biological Chemistry 287*, 8561–8570.

(*119*) Tang, W. K., and Xia, D., (Dec. 2013). Altered Intersubunit Communication Is the Molecular Basis for Functional Defects of Pathogenic p97 Mutants. *Journal of Biological Chemistry 288*, 36624–36635.

(*120*) Ju, J. S., and Weihl, C. C., (Apr. 2010). Inclusion body myopathy, Paget's disease of the bone and fronto-temporal dementia: a disorder of autophagy. *Human Molecular Genetics 19*, R38–R45.

(*121*) Schuetz, A. K., and Kay, L. E., (Nov. 2016). A Dynamic molecular basis for malfunction in disease mutants of p97/VCP. *eLife 5*.

(*122*) Schütz, A. K., Rennella, E., and Kay, L. E., (Aug. 2017). Exploiting conformational plasticity in the AAA+ protein VCP/p97 to modify function. *Proceedings of the National Academy of Sciences 114*, E6822–E6829.

(*123*) Huang, R., Ripstein, Z. A., Rubinstein, J. L., and Kay, L. E., (Jan. 2019). Cooperative subunit dynamics modulate p97 function. *Proceedings of the National Academy of Sciences 116*, 158–167.

(*124*) Tang, W. K., Zhang, T., Ye, Y., and Xia, D., (Dec. 2017). Structural basis for nucleotide-modulated p97 association with the ER membrane. *Cell Discovery 3*, 17045.

(*125*) Fernández-Sáiz, V., and Buchberger, A., (June 2010). Imbalances in p97 co-factor interactions in human proteinopathy. *EMBO reports 11*, 479–485.

(*126*) Arhzaouy, K., Papadopoulos, C., Schulze, N., Pittman, S. K., Meyer, H., and Weihl, C. C., (Jan. 2019). VCP maintains lysosomal homeostasis and TFEB activity in differentiated skeletal muscle. *Autophagy*, 1–18.

(*127*) Rabouille, C., Kondo, H., Newman, R., Hui, N., Freemont, P., and Warren, G., (1998). Syntaxin 5 is a common component of the NSF-and p97-mediated reassembly pathways of Golgi cisternae from mitotic Golgi fragments in vitro. *Cell 92*, 603–610.

(*128*) Yuan, X., Simpson, P., Mckeown, C., Kondo, H., Uchiyama, K., Wallis, R., Dreveny, I., Keetch, C., Zhang, X., Robinson, C., et al. (2004). Structure, dynamics and interactions of p47, a major adaptor of the AAA ATPase, p97. *The EMBO journal 23*, 1463–1473.

(*129*) Hänzelmann, P., and Schindelin, H., (Jan. 2016). Characterization of an Additional Binding Surface on the p97 N-Terminal Domain Involved in Bipartite Cofactor Interactions. *Structure 24*, 140–147.

(*130*) Isaacson, R. L., Pye, V. E., Simpson, P., Meyer, H. H., Zhang, X., Freemont, P. S., and Matthews, S., (July 2007). Detailed Structural Insights into the p97-Npl4-Ufd1 Interface. *Journal of Biological Chemistry 282*, 21361–21369.

(*131*) Park, S., Isaacson, R., Kim, H. T., Silver, P. A., and Wagner, G., (July 2005). Ufd1 Exhibits the AAA-ATPase Fold with Two Distinct Ubiquitin Interaction Sites. *Structure 13*, 995–1005.

(*132*) Yin, J., Lin, A. J., Golan, D. E., and Walsh, C. T., (2006). Site-specific protein labeling by Sfp phosphopantetheinyl transferase. *Nature Protocols 1*, 280–285.

(*133*) Chia, W. S., Chia, D. X., Rao, F., Bar Nun, S., and Geifman Shochat, S., (Dec. 2012). ATP Binding to p97/VCP D1 Domain Regulates Selective Recruitment of Adaptors to Its Proximal N-Domain. *PLoS ONE 7*, ed. by Kursula, I., e50490.

(*134*) Zhang, Z., Wang, Y., Li, C., Shi, Z., Hao, Q., Wang, W., Song, X., Zhao, Y., Jiao, S., and Zhou, Z., (Aug. 2015). The Transitional Endoplasmic Reticulum ATPase p97 Regulates the Alternative Nuclear Factor NF-kappaB Signaling via Partial Degradation of the NF-kappaB Subunit p100. *Journal of Biological Chemistry 290*, 19558–19568.

(*135*) Theile, C. S., Witte, M. D., Blom, A. E. M., Kundrat, L., Ploegh, H. L., and Guimaraes, C. P., (Sept. 2013). Site-specific N-terminal labeling of proteins using sortase-mediated reactions. *Nature Protocols 8*, 1800–1807.

(*136*) Bulfer, S. L., Chou, T.-F., and Arkin, M. R., (Aug. 2016). p97 Disease Mutations Modulate Nucleotide-Induced Conformation to Alter Protein–Protein Interactions. *ACS Chemical Biology 11*, 2112–2116.

(*137*) Rao, M. V., Williams, D. R., Cocklin, S., and Loll, P. J., (Nov. 2017). Interaction between the AAA+ ATPase p97 and its cofactor ataxin3 in health and disease: Nucleotide-induced conformational changes regulate cofactor binding. *Journal of Biological Chemistry 292*, 18392–18407.

(*138*) Tang, W. K., Li, D., Li, C.-c., Esser, L., Dai, R., Guo, L., and Xia, D., (July 2010). A novel ATP-dependent conformation in p97 N-D1 fragment revealed by crystal structures of disease-related mutants. *The EMBO journal 29*, 2217–2229.

(*139*) Mori-Konya, C., Kato, N., Maeda, R., Yasuda, K., Higashimae, N., Noguchi, M., Koike, M., Kimura, Y., Ohizumi, H., Hori, S., and Kakizuka, A., (Apr. 2009). p97/valosin-containing protein (VCP) is highly modulated by phosphorylation and acetylation. *Genes to Cells 14*, 483–497.

(*140*) Cloutier, P., Lavallée-Adam, M., Faubert, D., Blanchette, M., and Coulombe, B., (Jan. 2013). A Newly Uncovered Group of Distantly Related Lysine Methyltransferases Preferentially Interact with Molecular Chaperones to Regulate Their Activity. *PLoS Genetics 9*, ed. by Barsh, G. S., e1003210.

(*141*) Blythe, E. E., Olson, K. C., Chau, V., and Deshaies, R. J., (May 2017). Ubiquitin- and ATP-dependent unfoldase activity of P97/VCP•NPLOC4•UFD1L is enhanced by a mutation that causes multisystem proteinopathy. *Proceedings of the National Academy of Sciences 114*, E4380–E4388.

(*142*) Ye, Y., (Oct. 2006). Diverse functions with a common regulator: Ubiquitin takes command of an AAA ATPase. *Journal of Structural Biology 156*, 29–40.

(*143*) Johnson, E. S., Bartel, B., Seufert, W., and Varshavsky, A., (1992). Ubiquitin as a degradation signal. *The EMBO journal 11*, 497.

(*144*) Bachmair, A., Finley, D., and Varshavsky, A., (1986). In vivo half-life of a protein is a function of its amino-terminal residue. *Science 3018930*, 234.

(*145*) Wójcik, C., Rowicka, M., Kudlicki, A., Nowis, D., McConnell, E., Kujawa, M., and DeMartino, G. N., (2006). Valosin-containing protein (p97) is a regulator of endoplasmic reticulum stress and of the degradation of N-end rule and ubiquitin-fusion degradation pathway substrates in mammalian cells. *Molecular biology of the cell 17*, 4606–4618.

(*146*) Ballar, P., Shen, Y., Yang, H., and Fang, S., (Nov. 2006). The Role of a Novel p97/Valosin-containing Protein-interacting Motif of gp78 in Endoplasmic Reticulum-associated Degradation. *Journal of Biological Chemistry 281*, 35359–35368.

(*147*) Fang, S., Ferrone, M., Yang, C., Jensen, J. P., Tiwari, S., and Weissman, A. M., (2001). The tumor autocrine motility factor receptor, gp78, is a ubiquitin protein ligase implicated in degradation from the endoplasmic reticulum. *Proceedings of the National Academy of Sciences 98*, 14422–14427.

(*148*) Dong, K. C., Helgason, E., Yu, C., Phu, L., Arnott, D. P., Bosanac, I., Compaan, D. M., Huang, O. W., Fedorova, A. V., Kirkpatrick, D. S., Hymowitz, S. G., and Dueber, E. C., (Aug. 2011). Preparation of Distinct Ubiquitin Chain Reagents of High Purity and Yield. *Structure 19*, 1053–1063.

(*149*) Martinez-Fonts, K., and Matouschek, A., (Mar. 2016). A Rapid and Versatile Method for Generating Proteins with Defined Ubiquitin Chains. *Biochemistry 55*, 1898–1908.

(*150*) Fenton, W. A., Kashi, Y., Furtak, K., and Horwich, A. L., (Oct. 1994). Residues in chaperonin GroEL required for polypeptide binding and release. *Nature 371*, 614–619.

(*151*) Bandau, S., Knebel, A., Gage, Z. O., Wood, N. T., and Alexandru, G., (2012). UBXN7 docks on neddylated cullin complexes using its UIM motif and causes HIF1alpha accumulation. *BMC biology 10*, 1.

(*152*) Dai, R. M., and Li, C. C., (Aug. 2001). Valosin-containing protein is a multi-ubiquitin chain-targeting factor required in ubiquitin-proteasome degradation. *Nature Cell Biology 3*, 740–744.

(*153*) Rothballer, A., Tzvetkov, N., and Zwickl, P., (Mar. 2007). Mutations in p97/VCP induce unfolding activity. *FEBS Letters 581*, 1197–1201.

(*154*) Barthelme, D., and Sauer, R. T., (Feb. 2013). Bipartite determinants mediate an evolutionarily conserved interaction between Cdc48 and the 20 *S* peptidase. *Proceedings of the National Academy of Sciences 110*, 3327–3332.

(*155*) Xu, P., Duong, D. M., Seyfried, N. T., Cheng, D., Xie, Y., Robert, J., Rush, J., Hochstrasser, M., Finley, D., and Peng, J., (Apr. 2009). Quantitative Proteomics Reveals the Function of Unconventional Ubiquitin Chains in Proteasomal Degradation. *Cell 137*, 133–145.

(*156*) Zhang, Z., Lv, X., Yin, W.-c., Zhang, X., Feng, J., Wu, W., Hui, C.-c., Zhang, L., and Zhao, Y., (June 2013). Ter94 ATPase Complex Targets K11-Linked Ubiquitinated Ci to Proteasomes for Partial Degradation. *Developmental Cell 25*, 636–644.

(*157*) Schuberth, C., and Buchberger, A., (Oct. 2005). Membrane-bound Ubx2 recruits Cdc48 to ubiquitin ligases and their substrates to ensure efficient ER-associated protein degradation. *Nature Cell Biology 7*, 999–1006.

(*158*) Song, C., Wang, Q., Song, C., and Rogers, T. J., (July 2015). Valosin-containing protein (VCP/p97) is capable of unfolding polyubiquitinated proteins through its ATPase domains. *Biochemical and Biophysical Research Communications 463*, 453–457.

(*159*) Thoms, S., (2002). Cdc48 can distinguish between native and non-native proteins in the absence of cofactors. *FEBS letters 520*, 107–110.

(*160*) Carvalho, A. F., Pinto, M. P., Grou, C. P., Vitorino, R., Domingues, P., Yamao, F., Sá-Miranda, C., and Azevedo, J. E., (July 2012). High-Yield Expression in Escherichia coli and Purification of Mouse Ubiquitin-Activating Enzyme E1. *Molecular Biotechnology 51*, 254–261.

(*161*) McKinney, S. A., Murphy, C. S., Hazelwood, K. L., Davidson, M. W., and Looger, L. L., (Feb. 2009). A bright and photostable photoconvertible fluorescent protein. *Nature Methods 6*, 131–133.

(*162*) Zhang, M., Chang, H., Zhang, Y., Yu, J., Wu, L., Ji, W., Chen, J., Liu, B., Lu, J., Liu, Y., Zhang, J., Xu, P., and Xu, T., (July 2012). Rational design of true monomeric and bright photoactivatable fluorescent proteins. *Nature Methods 9*, 727–729.

(*163*) Bodnar, N. O., and Rapoport, T. A., (May 2017). Molecular Mechanism of Substrate Processing by the Cdc48 ATPase Complex. *Cell 169*, 722–735.e9.

(*164*) Olszewski, M. M., Williams, C., Dong, K. C., and Martin, A., (Dec. 2019). The Cdc48 unfoldase prepares well-folded protein substrates for degradation by the 26S proteasome. *Communications Biology 2*, 29.

(*165*) Weith, M., Seiler, J., van den Boom, J., Kracht, M., Hülsmann, J., Primorac, I., del Pino Garcia, J., Kaschani, F., Kaiser, M., Musacchio, A., Bollen, M., and Meyer, H., (Nov. 2018). Ubiquitin-Independent Disassembly by a p97 AAA-ATPase Complex Drives PP1 Holoenzyme Formation. *Molecular Cell 72*, 766–777.e6.

(*166*) Ewens, C. A., Kloppsteck, P., Förster, A., Zhang, X., and Freemont, P. S., (Feb. 2010). Structural and functional implications of phosphorylation and acetylation in the regulation of the AAA+ protein p97. *Biochemistry and Cell Biology 88*, 41–48.

(*167*) Li, J.-M., Wu, H., Zhang, W., Blackburn, M. R., and Jin, J., (Feb. 2014). The p97-UFD1L-NPL4 Protein Complex Mediates Cytokine-Induced IkappaBalpha Proteolysis. *Molecular and Cellular Biology 34*, 335–347.

(*168*) Dai, R.-M., Chen, E., Longo, D. L., Gorbea, C. M., and Li, C.-C. H., (1998). Involvement of Valosin-containing Protein, an ATPase Co-purified with IkBa and 26 S Proteasome, in Ubiquitin-Proteasome-mediated Degradation of IkBa. *Journal of Biological Chemistry 273*, 3562–3573.

(*169*) Ritson, G. P., Custer, S. K., Freibaum, B. D., Guinto, J. B., Geffel, D., Moore, J., Tang, W., Winton, M. J., Neumann, M., Trojanowski, J. Q., Lee, V. M.-. Y., Forman, M. S., and Taylor, J. P., (June 2010). TDP-43 Mediates Degeneration in a Novel Drosophila Model of Disease Caused by Mutations in VCP/p97. *Journal of Neuroscience 30*, 7729–7739.

(*170*) Reitsma, J. M., Liu, X., Reichermeier, K. M., Moradian, A., Sweredoski, M. J., Hess, S., and Deshaies, R. J., (Nov. 2017). Composition and Regulation of the Cellular Repertoire of SCF Ubiquitin Ligases. *Cell 171*, 1326–1339.e14.

(*171*) Gillen, C. M., and Forbush, B., (Feb. 1999). Functional interaction of the K-Cl cotransporter (KCC1) with the Na-K-Cl cotransporter in HEK-293 cells. *American Journal of Physiology-Cell Physiology 276*, C328–C336.

(*172*) Kirchner, P., Bug, M., and Meyer, H., (Mar. 2013). Ubiquitination of the N-terminal Region of Caveolin-1 Regulates Endosomal Sorting by the VCP/p97 AAA-ATPase. *Journal of Biological Chemistry 288*, 7363–7372.